Hindawi
Structural Control and Health Monitoring
Volume 2023, Article ID 9343343, 25 pages
https://doi.org/10.1155/2023/9343343

Research Article

A Real-Time Monitoring System for Cable Tension with Vibration Signals Based on an Automated Algorithm to Sieve Out Reliable Modal Frequencies

Wen-Hwa Wu, Chien-Chou Chen, Shang-Li Lin, and Gwolong Lai

Department of Civil and Construction Engineering, National Yunlin University of Science and Technology, Yunlin 640, Taiwan

Correspondence should be addressed to Wen-Hwa Wu; wuwh@yuntech.edu.tw

Received 29 December 2022; Revised 24 April 2023; Accepted 1 June 2023; Published 11 July 2023

Academic Editor: Hoon Sohn

Cables or suspenders are the critical force-transmitting components of cable-supported bridges, and their timely tension monitoring is consequently the most important issue in the corresponding structural health monitoring. However, very few works regarding the full automation of vibration-based tension estimation have been reported in the literature. To develop a monitoring system of cable tension based on real-time vibration signals, this research first employs an efficient stochastic subspace identification (SSI) method with tailored parameter selection to continuously identify the three frequencies of adjacent modes for the cables of Mao-Luo-Hsi Bridge. More importantly, an automated sieving algorithm is delicately established to obtain the stable modal frequencies by making the best of the specific modal frequency distribution for cables. The ratios between the frequency values identified from SSI analysis are exhaustively checked to systematically extract the qualified cable frequencies and decide their corresponding mode orders. The tension is finally computed with one available cable frequency according to the priority order predetermined by the statistics of identification rate. Demonstrated by analyzing the vibration signals measured from the stay cable of Mao-Luo-Hsi Bridge in real time for two full years, the effectiveness and robustness of this real-time monitoring system have been extensively testified. The long-term success rates for the immediate determination of dependable tension are found to be perfect for 15 of the 18 investigated cables. As for the other three cables, their corresponding success rates are still higher than 99.99% with very few cases of absent or false tension values.

1. Introduction

Cable-supported bridges generally include suspension bridges, cable-stayed bridges, and through-type arch bridges. Due to the demand for longer spans and aesthetic consideration, these types of bridges have become increasingly popular worldwide to rise as the mainstream in modern bridge engineering. Cables or suspenders are the critical force-transmitting components of those cable-supported bridges, and their timely tension monitoring is consequently the most important issue in the corresponding structural health monitoring (SHM). The sudden collapse of Nan-Fang-Ao Bridge occurred in Taiwan in 2019 can be taken as a typical example. Such a tragic accident caused the casualties of six deaths and twelve injured people together with heavy damage of three fishing vessels and one tank truck. The suspenders of this arch bridge successively broke in a very short time to result in the loss of suspension for the main bridge girder and its subsequent fall into the water. After the cruel lessons learned from the incident of Nan-Fang-Ao Bridge, much more resources from the central and local governments of Taiwan have since been invested to conduct extensive inspection and SHM of cable-supported bridges.

In practical tension estimation and monitoring, the ambient vibration method [1–3] is most commonly employed because of its expedient operation and the unsophisticated analysis benefiting from the one-dimensional geometry of cable. Application of the vibration-based tension estimation method typically starts with identifying the modal frequencies of a cable from its ambient vibration measurements and then calculates the cable tension based on an analytical formula requiring at least a cable frequency, the

given vibration length, and its mass per unit length. More involved effects such as flexural rigidity [4, 5] and gravity sag [6, 7] have also been well studied in the literature to improve the accuracy of this method. Nevertheless, the rubber constraints and special anchorage systems are normally designed near the boundaries of modern cables. These devices can unfriendly obstruct the accurate determination of their vibration lengths and lead to non-negligible errors in tension estimation. To tackle this difficulty and avoid the troubles of complex modelling in the neighborhood of cable boundaries, a new methodology has been first propelled and systematically developed by the authors [8–12]. An original idea was adopted in those studies to directly obtain the effective vibration lengths for desired modes by further combining the information of mode shapes. Collection of multiple synchronized measurements on a cable is required in this method for the identification of mode shape values at different sensor locations. The effective vibration length corresponding to each interested mode can then be independently attained by optimally fitting the sinusoidal component of the mode shape. With the identified modal frequencies and the determined effective vibration lengths for a few selected modes, the cable tension and flexural rigidity are eventually solved by simple linear regression techniques. This innovative method has so far been applied to conduct the cable tension estimation for more than 30 cable-supported bridges in Taiwan. A number of other researchers have also joined to explore the same concept of effective vibration length [13–15].

Following the galloping progress of sensor technology in recent years, much more cable-supported bridges have been equipped with permanent vibration sensors on their cables to carry out real-time and long-term tension monitoring. For establishing an accurate cable tension monitoring system, it needs to conduct the abovementioned method based on multiple vibration measurements only once in the initial stage. With the corresponding effective vibration lengths determined, one sensor installed on each cable would be adequate to supply the vibration measurement, from which the cable frequencies can be immediately identified for continuous tension monitoring. Under normal operating conditions of bridges, it is usually sufficient to accurately identify the modal frequencies of cables by applying the conventional discrete Fourier transform (DFT) technique. To achieve real-time monitoring in practical applications, however, the continuously stable identification of cable frequencies becomes a great challenge. The ambient vibration signals can be very weak and highly polluted by noise during the hours without traffic. Accordingly, a more resilient modal identification method with its guaranteed performance is necessary in such long-term operations.

Operational modal analysis (OMA) has been well advanced in the past few decades to yield several robust algorithms for obtaining reliable modal parameters simply from the collected output signals. Among all these methods, stochastic subspace identification (SSI) may attract the most popular applications on civil engineering structures [16–19]. This technique has been successfully practiced for the long-term SHM of historical architectures [20, 21], arch dams [22], skyscrapers [23, 24], and long-span bridges [25, 26]. In these cases, a regularly encountered problem is that different values of the time lag parameter and the system order parameter prescribed in SSI analysis would produce varied modal parameters. The conventional stabilization diagram and proper discrimination criteria according to theories like clustering analysis [27–29] have been established to deal with such a difficulty.

During the past decade, the development is further focused on automated SSI approaches that are capable of processing large datasets from long-term monitoring systems without the need of human interventions [30–32]. Particularly in the last few years, many efforts have been made to accomplish automatic SSI-based monitoring. Zonno et al. [33] proposed a multistage methodology combining the data-driven SSI together with the techniques of hierarchical clustering and adaptive modal tracking for the automatic modal parameter identification of historical buildings in Portugal and Peru. Li et al. [34] developed a three-stage automated algorithm by incorporating the second-order blind identification with the covariance-driven SSI to conduct continuous monitoring for a concrete arch gravity dam in China. Sadeqi et al. [35] established an automated procedure integrating a simplified SSI algorithm in conjunction with the statistical feature extraction of identified modal parameters. In this research, three years of continuous data from a modern tower in Iran were processed to effectively perform its SHM. Sun et al. [36] used a multistage clustering approach by defining the hierarchical clustering threshold to handle the results from the covariance-driven SSI and automatically identify the modal parameters of a cable-stayed bridge in Australia. Zhang et al. [37] lately amalgamated a fast density peak clustering algorithm with the covariance-driven SSI to automatically select the appropriate structural modes from the stabilization diagram and applied it to a cable-stayed bridge in China.

After the abovementioned accident of Nan-Fang-Ao Bridge, the authors earned an opportunity to help develop a real-time tension monitoring system based on the vibration signals of Mao-Luo-Hsi Bridge that will be introduced in the next section. While a few new techniques [38–40] were recently suggested to effectively identify the time-varying cable tension, very few works regarding the full automation of vibration-based tension estimation have been reported in the literature. Jin et al. [41] first applied a modified automatic multiscale-based peak detection algorithm on the power spectral density function. The median absolute deviation following baseline corrections is then determined to extract the modal frequencies of cables for autonomous tension monitoring. Jeong et al. [42] constructed an automated cable tension monitoring system by proposing a fully automated peak-picking algorithm using a region-based convolution neural network. Even so, only short durations of vibration data from real stay cables were tested in these two recent studies to demonstrate the effectiveness of their proposed methods. No long-term results were actually presented to unambiguously verify the feasibility of a totally automatic cable tension monitoring system in practice.

Enhanced with an alternative stabilization diagram and a hierarchical sifting process, a novel covariance-driven SSI methodology was also proposed in a recent work by the authors [43]. In addition to its original application in stay cables [43], this improved SSI algorithm has been further demonstrated to sturdily identify accurate modal parameters of cable-stayed bridges [44] and office buildings [45, 46] from long-term vibration measurements. On the basis of employing such an effective SSI algorithm to continuously identify the modal frequencies, a real-time tension monitoring system is developed and applied to the cables of Mao-Luo-Hsi Bridge. In long-term SHM, the occurrence of abnormal signals due to various possible sources is virtually inevitable and may significantly obstruct the subsequent analyses. The first phase of this tension monitoring system aimed to automatically detect and process the signal anomaly of cable vibration measurements has been reported in a recent article [47]. The current paper will focus on elaborating the most critical ingredient of the tension monitoring system, which is an automated algorithm innovatively created to robustly sieve out the stable modal frequencies of the cable based on the characteristic of their steady ratios. Furthermore, the real-time cable tension monitoring results of Mao-Luo-Hsi Bridge for a long duration of two years will be also presented to solidly attest the robustness and performance of the developed tension monitoring system in real applications.

2. Mao-Luo-Hsi Bridge and Its Cable Vibration Measurements

With its photo displayed in Figure 1(a), Mao-Luo-Hsi Bridge transverses Mao-Luo River to connect National Highway 3 and the east end of Bagua Mountain Tunnel. Open to traffic since 2002, this bridge has been serving as a main artery between the two towns of Yuanlin of Changhua County and Caotun of Nantou County in Central Taiwan. It is an unsymmetrical single-pylon cable-stayed bridge containing a main span with a length of 119 m and a side span with a length of 51 m, both built with steel box girders. A steel arch crossing over the bridge deck and with a height of 60 m is adopted as its pylon. As illustrated in Figure 1(c), the cable system of Mao-Luo-Hsi Bridge contains four cable planes and each plane is composed of nine stay cables arranged in the unsymmetrical fan shape. With their lengths ranging from 27.2 m to 103.1 m, these 36 cables are numbered in triple digits according to the following rules: (a) the first digit indicates the number of the belonged cable plane; (b) the last two digits label the cables of each plane in ascending order from the Yuanlin side to the Caotun side; (c) the two main cables near the Yuanlin side (or Bagua Mountain Tunnel) are anchored into a concrete block outside the main girder and postfixed with a and b, respectively. The design length, angle of inclination, and number of parallel steel strands (15.2 mm in diameter) for the cables in the first two cable planes are listed in Table 1 for reference. It should be noticed that all the steel strands of each stay cable are encased in a high-density polyethylene (HDPE) tube, but no grouting material is filled between them. A typical cable cross section is depicted in Figure 1(b), and the mass per unit length for each cable is also listed in Table 1 by considering both the steel strands and the HDPE tube.

To ensure the structural safety of Mao-Luo-Hsi Bridge, an SHM system was installed by the Directorate General of Highways and started its operation in November of 2020. The permanent sensors deployed on the bridge include one anemometer, 11 temperature sensors, one seismograph, one biaxial inclinometer, two displacement transducers, seven settlement gauges, 16 strain gauges, and 36 accelerometers. The detailed description given here will be limited to the accelerometers which are directly relevant to the investigation of this study. On each stay cable, one force balance accelerometer SA-10 produced by Sara Electronic Instruments in Italy was installed at the position around 5 m high above the deck to continuously conduct its in-plane acceleration measurements. For the convenience of timely cable tension monitoring, the monitoring system is designed to output the measured acceleration signals for all cables every 15 minutes and then store them into a separate data file for subsequent analyses. Therefore, it would generate 96 measurement data files every day for each stay cable to attain real-time tension monitoring.

3. Identification of Cable Frequencies with Stochastic Subspace Methodology

Multiple vibration measurements on each cable of Mao-Luo-Hsi Bridge were conducted in the initial stage to decide its flexural rigidity and effective vibration lengths for the dominant modes [8–12]. It was found that the identified flexural rigidity of each cable is consistently larger than the lower limit estimated by considering a circular cross section with an area equal to the sum of all its strands. Besides, the corresponding values for different cables follow the same order as that sorted by their numbers of steel strands. Both tendencies certify that the cable's flexural rigidity such determined is reasonable and can be confidently used as a known parameter in long-term monitoring. Merely one modal frequency is required to estimate the real-time tension value for each cable with the given flexural rigidity and effective vibration length. The SSI methodology recently developed by the authors [43–46] is employed in the current work aimed to continuously identify three cable frequencies of adjacent modes. Such a strategy is adopted to guarantee the identification of at least one cable frequency at any time considering the wide variability possibly occurring in long-term monitoring. This SSI algorithm is succinctly reviewed in the first subsection. Based on the preliminary analysis with one week of cable vibration measurements for Mao-Luo-Hsi Bridge before the official operation of its SHM system, discussions on the determination of frequency range and the selection of SSI parameters are also presented in the second and third subsections.

3.1. Alternative Stabilization Diagram and Hierarchical Shifting Process. The improved SSI algorithm follows the covariance-driven approach, which generally starts from the

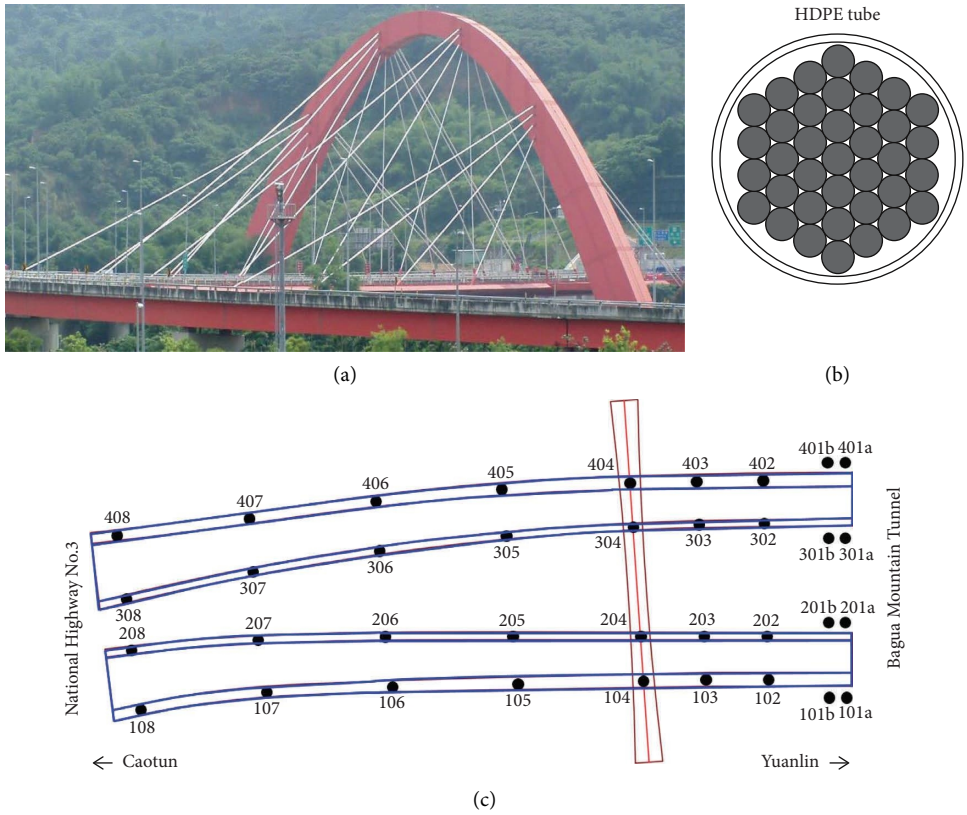

Figure 1: Mao-Luo-Hsi Bridge and its cable system. (a) Photo. (b) Cross section of cable. (c) Cable arrangement.

Table 1: Basic parameters for cables in the first two cable planes of Mao-Luo-Hsi Bridge.

Cable number	Design length (m)	Angle of inclination (°)	Number of steel strands	Mass per unit mass (kg/m)
101a	60.516	34.2	73	85.371
101b	60.526	34.2	73	85.371
102	43.682	40.7	61	72.159
103	32.603	59.4	37	45.735
104	27.827	90.0	37	45.735
105	37.080	48.8	37	45.735
106	54.963	31.2	61	72.159
107	76.409	23.2	61	72.159
108	97.426	18.5	61	72.159
201a	70.348	43.5	73	85.371
201b	70.312	43.5	73	85.371
202	54.906	51.5	61	72.159
203	45.987	67.5	37	45.735
204	42.880	90.0	37	45.735
205	48.296	61.3	37	45.735
206	62.691	43.1	61	72.159
207	81.610	32.4	61	72.159
208	102.697	25.6	61	72.159

state space description for a linear dynamic system with n degrees of freedom (DOF). It assumed that the output measurements for such a system are conducted using the sampling time increment Δt to have the $l \times 1$ output vector $\mathbf{y}(j)$ at the time instant $j\Delta t$. The output vectors measured at M consecutive time instants $(j = 0, 1, 2, \cdots\cdots, M-1)$

can then be systematically arranged into a Hankel matrix by selecting a time lag parameter i:

$$\mathbf{Y}_{0|2i-1} = \frac{1}{\sqrt{h}} \left[\begin{array}{cccc} \mathbf{y}(0) & \mathbf{y}(1) & \cdots & \mathbf{y}(h-1) \\ \mathbf{y}(1) & \mathbf{y}(2) & \cdots & \mathbf{y}(h) \\ \vdots & \vdots & \ddots & \vdots \\ \mathbf{y}(i-1) & \mathbf{y}(i) & \cdots & \mathbf{y}(i+h-2) \\ \hline \mathbf{y}(i) & \mathbf{y}(i+1) & \cdots & \mathbf{y}(i+h-1) \\ \mathbf{y}(i+1) & \mathbf{y}(i+2) & \cdots & \mathbf{y}(i+h) \\ \vdots & \vdots & \ddots & \vdots \\ \mathbf{y}(2i-1) & \mathbf{y}(2i) & \cdots & \mathbf{y}(2i+h-2) \end{array} \right]_{2il \times h} = \left[\begin{array}{c} \mathbf{Y}_{0|i-1} \\ \hline \mathbf{Y}_{i|2i-1} \end{array} \right] = \left[\begin{array}{c} \mathbf{Y}_p \\ \hline \mathbf{Y}_f \end{array} \right], \tag{1}$$

where $\mathbf{Y}_p$ and $\mathbf{Y}_f$ are both $il \times h$ with $h = M - 2i + 1$. Multiplication of the two equally divided submatrices $\mathbf{Y}_p$ and $\mathbf{Y}_f$ of the Hankel matrix would result in the approximation of the so-called Toeplitz matrix $\mathbf{T}$. Singular value decomposition (SVD) of $\mathbf{T}$ can next be carried out to obtain

$$\begin{aligned} \mathbf{T} \approx \mathbf{Y}_f \mathbf{Y}_p^T = \mathbf{U}\mathbf{S}\mathbf{V}^T &= \left[\begin{array}{cc} (\mathbf{U}_1)_{il \times 2n} & (\mathbf{U}_2)_{il \times n_1} \end{array} \right] \left[\begin{array}{cc} (\mathbf{S}_1)_{2n \times 2n} & \mathbf{0}_{2n \times n_1} \\ \mathbf{0}_{n_1 \times 2n} & (\mathbf{S}_2)_{n_1 \times n_1} \approx \mathbf{0}_{n_1 \times n_1} \end{array} \right] \left[\begin{array}{c} \left(\mathbf{V}_1^T\right)_{2n \times il} \\ \left(\mathbf{V}_2^T\right)_{n_1 \times il} \end{array} \right] \\ &\approx \mathbf{U}_1 \mathbf{S}_1 \mathbf{V}_1^T, \end{aligned} \tag{2}$$

where $n_1 = il - 2n$, $\mathbf{U}$ and $\mathbf{V}$ are orthogonal matrices, and $\mathbf{S}$ is a quasi-diagonal matrix with positive diagonal elements sorted in a decreasing order. Further taking

$$\mathbf{O}_i = \mathbf{U}_1 \mathbf{S}_1^{1/2} \quad \text{and} \, \Gamma_i = \mathbf{S}_1^{1/2} \mathbf{V}_1^T, \tag{3}$$

then the discretized system matrix $\mathbf{A}$ in the state space can be solved by

$$\mathbf{A} = \mathbf{O}_i^{\oplus}(1\colon l(i-1), :)\mathbf{O}_i(l+1\colon li, :), \tag{4}$$

where $\oplus$ symbolizes the pseudo-inverse operation. According to the theory of linear systems, the modal frequencies ω_j's, the damping ratios ξ_j's, and the mode shape vectors at the output measurement locations $\boldsymbol{\varphi}_j$'s can be ultimately determined from the eigenvalues and eigenvectors of $\mathbf{A}$.

From the above review, it is evident that the time lag parameter i in equation (1) and the system order parameter n in equation (2) need to be specified in conducting the SSI analysis. A value no less than the number of physical modes within the interested frequency range is normally required for the system order parameter to ensure the incorporation of unambiguously contributing modes. As for the time lag parameter, the identified modal parameters should be insensitive to it if the excitation is close to the white noise and stationary assumptions on which the derivation of SSI is based. Consequently, the determination of modal parameters by the SSI technique is usually accompanied with the stabilization diagram to check the stability of the identified frequency values with the increasing value of n under a designated value of i. In applications of large-scale civil structures typically subjected to narrowly banded or non-stationary excitations, however, the performance of conventional stabilization diagrams may be significantly altered by different selections of the time lag parameter [16]. The authors [43] recently tackled such a difficulty by first establishing a threshold i_c of the time lag parameter to ensure stable identification results:

$$i \geq i_c = \frac{s}{F_1}, \tag{5}$$

where $s = 1/\Delta t$ denotes the sampling rate of measurement and F_1 signifies the fundamental frequency of structure. With the criterion of equation (5), an alternative stabilization diagram was then proposed by displaying the identified frequency values with the increasing value of i under a fixed value of n [43]. The lower limit $i_{\min}$ of the time lag parameter is suggested to be set as the critical threshold i_c presented in equation (5), and its upper limit $i_{\max}$ is decided by the need in the subsequent processes to extract reliable modal parameters.

Even with the construction of an alternative stabilization diagram, further efforts are needed to complete the task of automatically and consistently extracting clustered modal parameters from this diagram. A three-stage hierarchical sifting process in the order of modal frequency, damping ratio, and mode shape vector was additionally advanced by

the authors [43, 48]. The following review will simply focus on the first sifting stage because merely the modal frequencies are necessary for the estimation of the cable tension monitored in the current study. With the alternative stabilization diagram where the time lag parameter is increased from $i_{\min}$ to $i_{\max} = i_{\min} + \Delta i$, the conduction of SSI analysis for all these $\Delta i + 1$ cases would produce multiple sets of modal parameters:

$$\left(f_j, \xi_j, \boldsymbol{\varphi}_j\right), j = 1, 2, \cdots\cdots, N. \tag{6}$$

In equation (6), the modal frequency $f_j = \omega_j/2\pi$ is in the unit of Hz and N represents the total number of frequency values falling in the inspected frequency range. The first stage of the hierarchical sifting process begins with sorting all frequency values appearing in the stabilization diagram in ascending order:

$$f_1 \le f_2 \le \cdots\cdots \le f_N. \tag{7}$$

It is designed to conveniently extract the clustered frequency values for each mode using a simple clustering index:

$$\Delta f_j = f_{j+K-1} - f_j, = 1,2, \cdots\cdots, (N - K + 1), \tag{8}$$

to indicate the span of any adjacent K frequency values. The extraction of all locally clustered frequency values can then be easily accomplished by just looking for all local minima $\Delta f_{k_1}, \Delta f_{k_2}, \cdots\cdots, \Delta f_{k_r}$ from $\Delta f_1, \Delta f_2, \cdots\cdots, \Delta f_{N-K+1}$. Moreover, the condition

$$\Delta f_{k_j} \le \overline{\Delta f}, j = 1, 2, \cdots\cdots, r, \tag{9}$$

can be further checked to confirm that each extracted group of frequency values would satisfy a prescribed threshold of concentration.

3.2. Determination of Target Modes and Frequency Range. The improved SSI methodology reviewed in the previous subsection is applied in this research to conduct tension monitoring for stay cables. Theoretically, any modal frequency F_j can be used to estimate the cable tension by the following formula:

$$T = 4\overline{m}F_j^2\left(\frac{L_j}{j}\right)^2 - \frac{\pi^2 EI}{\left(L_j/j\right)^2}, j = 1, 2, 3, \cdots, \tag{10}$$

with predetermined effective vibration length L_j and flexural rigidity EI (E signifies Young's modulus and I stands for the cross-sectional area moment of inertia). But for long-term monitoring, the selection of a particular or a few stably identifiable modes needs to be made such that systematic operations can be implemented. Since the steady identification of three consecutive modal frequencies of a cable is aimed in the current work, the examined frequency range for each cable is determined by confidently covering its three chosen modal frequencies. In other words, a corresponding band-pass filter is exerted on the acceleration signal of each cable before conducting the SSI analysis.

With 7 days of cable measurements from 2020/10/21 to 2020/10/27, the characteristics of mode contribution for each cable are first investigated in this study to decide its three consecutive modes as the identification target and the corresponding frequency range. Taking Cables 107 and 201b as examples, 15 minutes of representative acceleration measurements for each cable as plotted in Figures 2(a) and 3(a) are extracted from this week to conduct Fourier transform. The corresponding Fourier amplitude spectra (FAS) are plotted in Figures 2(b) and 3(b). It is apparently demonstrated in these two figures that the modal frequencies of a stay cable regularly hold values approximately in integer multiples of its fundamental frequency and are accordingly easy to be distinguished. More importantly, the second, third, and fourth modes are the three most contributing modes with three highest peaks for both cables. The trend shown in Figures 2 and 3, however, is valid only for one data file including the selected 15 minutes of cable measurements. A complete picture can be more distinctly observed if the results for all 672 measurement data files from 2020/10/21 to 2020/10/27 are scrutinized. According to the peak values exhibited in the FAS of each 15-minute time interval, statistics of the three most dominantly contributing modes in one whole week are illustrated in Figure 4. For Cable 107, the percentage of its second mode to rank the first three is 22% + 25% + 19% = 66%, that of its third mode is 51% + 29% + 9% = 89%, and that of its fourth mode is 12% + 22% + 29% = 63%. Regarding Cable 201b, the percentage of its second mode to rank the first three is 65% + 22% + 7% = 94%, that of its third mode is 22% + 29% + 24% = 75%, and that of its fourth mode is 7% + 25% + 49% = 81%. All other modes of either Cable 107 or Cable 201b are with less percentage to rank the first three than the three modes listed above. Therefore, the best choice of three consecutive modes would be from the second to the fourth mode for both cables.

Based on the aforementioned statistics, the frequency range of the band-pass filter for each cable can be subsequently determined. As indicated in Figure 2(b) by the interval between two vertical red lines, the considered frequency range for Cable 107 is taken from $f_{\min} = 1.8$ Hz (roughly the middle value for the frequencies of the first and second modes) to $f_{\max} = 5.4$ Hz (approximately the middle value for the frequencies of the fourth and fifth modes). Likewise, the investigated frequency range for Cable 201b is also shown in Figure 3(b) between the two vertical red lines at 2.2 Hz and 6.5 Hz. The three consecutive modes and the frequency range selected for each cable in the first two cable planes of Mao-Luo-Hsi Bridge are listed in Table 2. It can be found from this table that the second to fourth modes are identically chosen for the longer cables labelled with 01a, 01b, 02, 06, 07, and 08 in each cable plane. On the other hand, the first to third modes are consistently picked for the shorter cables labelled with 03, 04, and 05 in each cable plane. Such a trend is the same for the cables in the other two cable planes, whose results are not comprehensively included in the current paper due to the limitation of length.

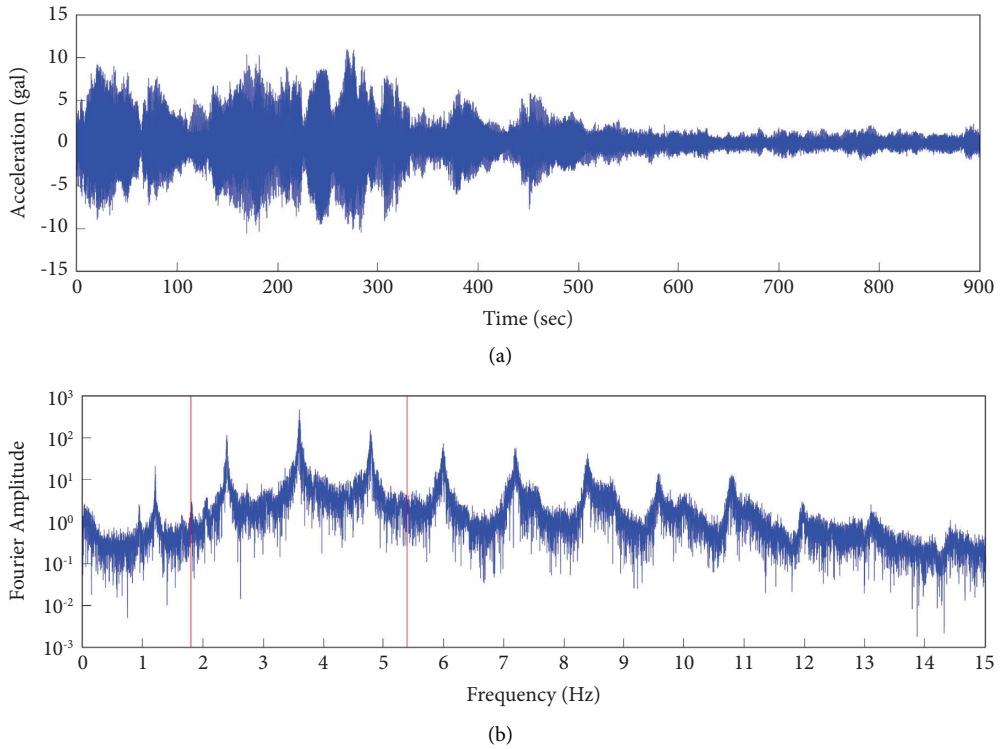

Figure 2: 15 minutes of time history and the corresponding Fourier amplitude spectrum for the acceleration measurement of Cable 107. (a) Time history. (b) Fourier amplitude spectrum.

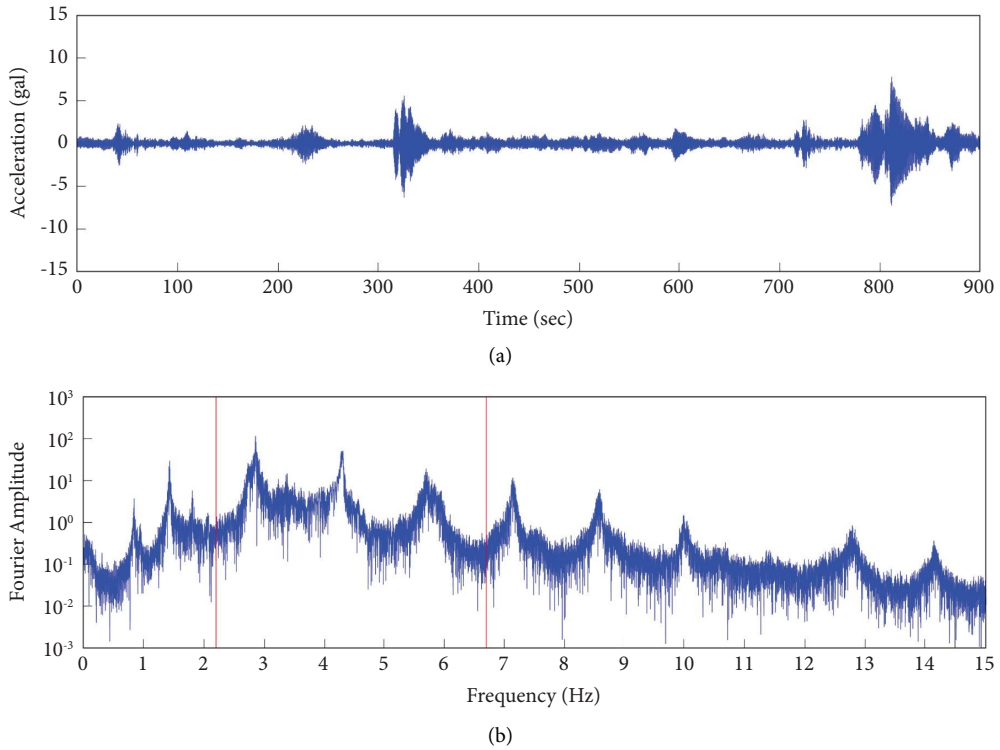

Figure 3: 15 minutes of time history and the corresponding Fourier amplitude spectrum for the acceleration measurement of Cable 201b. (a) Time history. (b) Fourier amplitude spectrum.

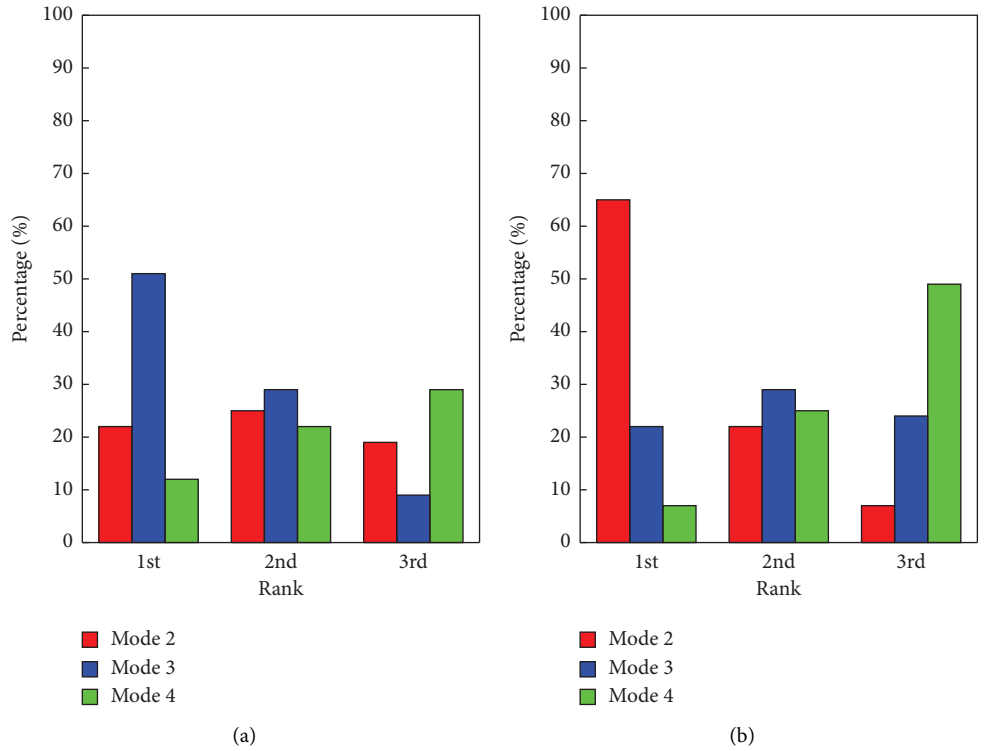

Figure 4: Statistics of the three most dominant modes for two cables in one week. (a) Cable 107. (b) Cable 201b.

Table 2: Adopted parameters of SSI analysis for cables in the first two cable planes.

Cable number	Frequency range (Hz)		Range of i		Value of n	Target modes (priority)		
	f_{min}	f_{max}	i_{min}	i_{max}		m_1	m_2	m_3
101a	2.3	6.9	130	230	3	2 (1st)	3 (3rd)	4 (2nd)
101b	2.2	6.6	140	240	3	2 (1st)	3 (3rd)	4 (2nd)
102	2.9	8.7	110	210	3	2 (1st)	3 (2nd)	4 (3rd)
103	1.5	10.4	70	170	3	1 (1st)	2 (2nd)	3 (3rd)
104	1.8	12.5	60	160	3	1 (2nd)	2 (1st)	3 (3rd)
105	1.6	10.8	70	170	3	1 (1st)	2 (2nd)	3 (3rd)
106	3.2	9.5	100	200	3	2 (1st)	3 (2nd)	4 (3rd)
107	1.8	5.4	170	270	3	2 (3rd)	3 (1st)	4 (2nd)
108	1.1	3.2	260	360	4	2 (1st)	3 (2nd)	4 (3rd)
201a	2.2	6.5	140	240	3	2 (1st)	3 (3rd)	4 (2nd)
201b	2.2	6.5	140	240	4	2 (1st)	3 (3rd)	4 (2nd)
202	2.3	7.1	130	230	3	2 (1st)	3 (2nd)	4 (3rd)
203	1.1	7.5	100	200	4	1 (1st)	2 (2nd)	3 (3rd)
204	1.2	8.5	90	190	3	1 (2nd)	2 (1st)	3 (3rd)
205	1.2	8.4	90	190	3	1 (1st)	2 (2nd)	3 (3rd)
206	2.6	7.8	120	220	4	2 (1st)	3 (2nd)	4 (3rd)
207	1.7	5.1	180	280	3	2 (3rd)	3 (1st)	4 (2nd)
208	1.0	3.0	280	380	4	2 (1st)	3 (2nd)	4 (3rd)

3.3. Parameter Selection for Real-Time SSI Analysis. Following the guidelines described in Section 3.1, the system order parameter n, the range of time lag parameter i, and the parameters for the first sifting stage are selected for the real-time SSI analysis of each cable. Inspecting the FAS for the measurement on Cable 107 exhibited in Figure 2(b), it is obvious that three prominent peaks corresponding to three consecutive cable modes appear in the examined frequency range between 1.8 Hz and 5.4 Hz. As a result, it is proper to fix the system order parameter at $n = 3$ in this case for establishing the alternative stabilization diagram. Further checking the FAS in Figure 3(b) obtained from the measurement on Cable 201b, there exist four noticeable peaks including one clearly not belonging to a cable mode. In this case, $n = 4$ would no doubt be an appropriate choice in constructing the alternative stabilization diagram for more

steady identification of three cable frequencies. It is noteworthy that higher values of n can actually be employed in these two cases to obtain stable identification as well. Nevertheless, more clustered frequency values associated with higher values of n in the alternative stabilization diagram would induce severer challenges to sieve out reliable cable frequencies as will be dealt with in the next section. Since the frequencies of three consecutive modes are targeted for each cable, the assigned value of $n = 3$ is the first priority taken in this study as long as three significant peaks are typically observed in its examined frequency range like the case of Cable 107. But for a few cases such as Cable 201b where additional peaks may also occur, the selection of $n = 4$ is found to be sufficient as will be seen in the next section.

With the fundamental frequency $F_1 \approx 1.2$Hz of Cable 107 and the sampling rate of measurement $s = 200$ Hz, the corresponding critical threshold can be determined from equation (5) to have $i_c = 200/1.2 \approx 170$. As for Cable 201b with its fundamental frequency $F_1 \approx 1.4$Hz, the critical threshold becomes $i_c = 200/1.4 \approx 140$. Hence, the SSI analysis for the measurement of Cable 107 shown in Figure 2(a) is performed with the time lag parameter increasing from $i_{\min} = 170$ to $i_{\max} = i_{\min} + \Delta i = 170 + 100 = 270$. The resulting alternative stabilization diagram can then be obtained and plotted in Figure 5(a) where the identified frequency values are symbolized by black cross signs with its corresponding FAS displayed in the grey background. In addition, the alternative stabilization diagram of Figure 6(a) for the measurement of Cable 201b illustrated in Figure 3(a) is constructed with $i_{\min} = 140$ and $i_{\max} = i_{\min} + \Delta i = 140 + 100 = 240$. Concerning the first stage of sifting with equations (7)–(9), $K = 51$ ($>0.5\Delta i$) and $\overline{\Delta f} = 0.05$ Hz are consistently taken for each cable to guarantee the quality of extracted frequency values. Using these two parameter values, three groups of clustered frequency values can be extracted from Figure 5(a) and four groups from Figure 6(a) as portrayed in Figures 5(b) and 6(b), respectively, by blue cross signs. As for the assigned values of n, $i_{\min}$, and $i_{\max}$ for all cables in the first two cable planes, they are also summarized in Table 2.

4. Automated Sieving Algorithm for Reliable Cable Frequencies

After going through the first stage of sifting, $K = 51$ survivors in each clustered group of Figure 5(b) for Cable 107 and of Figure 6(b) for Cable 201b can then be averaged to determine the eventually identified frequency value. Taking one day of measurement for Cable 107 on 2020/10/21 as an example, the results after conducting the SSI analysis on the 96 segments of 15-minute acceleration signal are depicted in Figure 7. Similarly, the corresponding results for the measurement of Cable 201b on 2020/10/22 are demonstrated in Figure 8. From Figure 7, it is transparent that three frequency values supposedly corresponding to Modes 2, 3, and 4 of Cable 107 with the assigned value of $n = 3$ in the SSI analysis can be steadily identified for each time interval with only one exception. At the time interval from 00:15 to 00:30, merely two frequency values corresponding to Modes 2 and 3 are obtained after the first stage of sifting. Among all 95 intervals with three identified frequency values, there is simply one frequency moderately deviated from the normal value of Mode 2 at the time interval from 01:15 to 01:30 and indicated by a red dot in Figure 7. As for the case of Cable 201b where $n = 4$ is adopted in the SSI analysis, Figure 8 reveals that four sifted frequency values are obtained in 44 intervals, three frequency values are identified in 48 intervals, and just two frequency values are gained in the other four intervals. In each interval with four sifted frequencies, there always exists one value surely not belonging to a cable mode and also indicated by a red dot. Besides, the correspondence to Modes 2, 3, and 4 of Cable 201b can be clearly found in all 48 intervals with three identified frequency values, and Mode 3 is typically missing in the four intervals with only two frequency values. Comparison of Figures 7 and 8 further suggests that the measurement from Cable 107 is more expedient for the conduction of SSI analysis than that from Cable 201b. But at all events, the frequency values not associated with the examined cable modes (the red dots shown in Figures 7 and 8) need to be effectively sieved out. In addition, the correct determination has to be made for the mode orders corresponding to the remaining cable frequencies. Taking advantage of the specific modal frequency distribution of cables, an automated sieving algorithm will be developed in this section to satisfy the above two essential features such that the accuracy and robustness of the subsequent cable tension estimation can be secured in long-term monitoring.

4.1. Difficulties and General Ideas. It may not seem complicated for human beings to pick out the anomalous red dots in Figures 7 and 8 and decide the mode orders corresponding to the three or fewer cable frequencies in each interval. To attain fully automatic cable tension monitoring, however, a comprehensive discrimination and classification algorithm has to be rigorously established. It should be especially pointed out that this task cannot be conveniently handled by simply setting a range of variation for each cable frequency. A wide range would not suit the purpose to effectively sieve out the frequency values not corresponding to cable modes such as the red dot in Figure 7. On the other hand, a narrow range may not reasonably cover the frequency variation induced by environmental factors such as temperature and live load. More importantly, the occurrence of bridge damage can lead to significant variations of cable tension and consequently substantial changes in cable frequency. Under such circumstances, it is nothing but fishing in the air to conduct the discrimination of cable frequencies based on a fixed range of variation.

The special characteristic for the modal frequencies of a stay cable to hold values close to an arithmetic sequence (particularly for the frequencies of lower modes where the

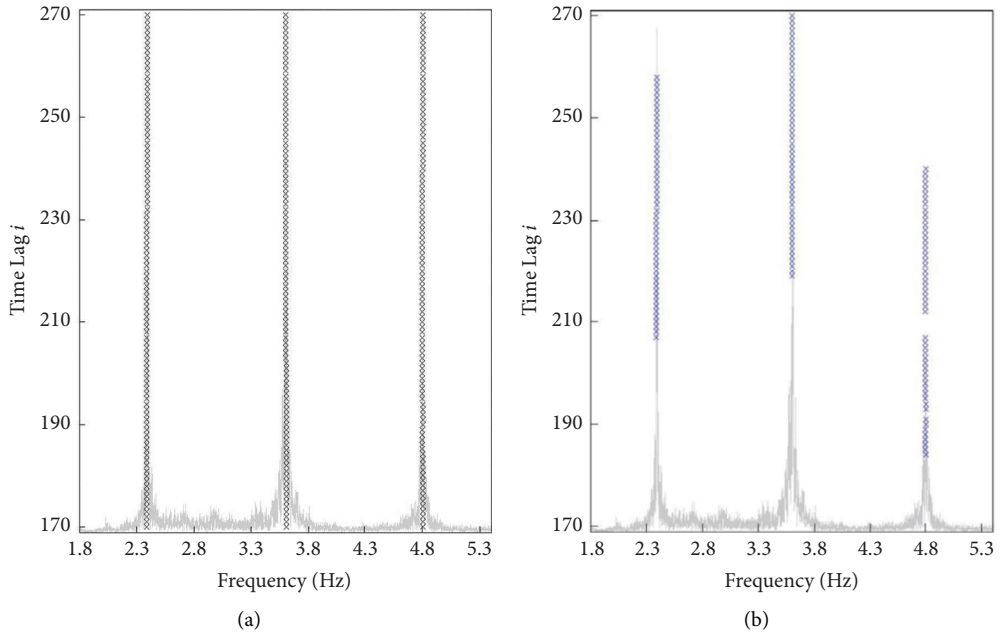

Figure 5: Alternative stabilization diagrams for SSI analysis of Cable 107 before and after the first sifting stage. (a) Before the first sifting stage. (b) After the first sifting stage.

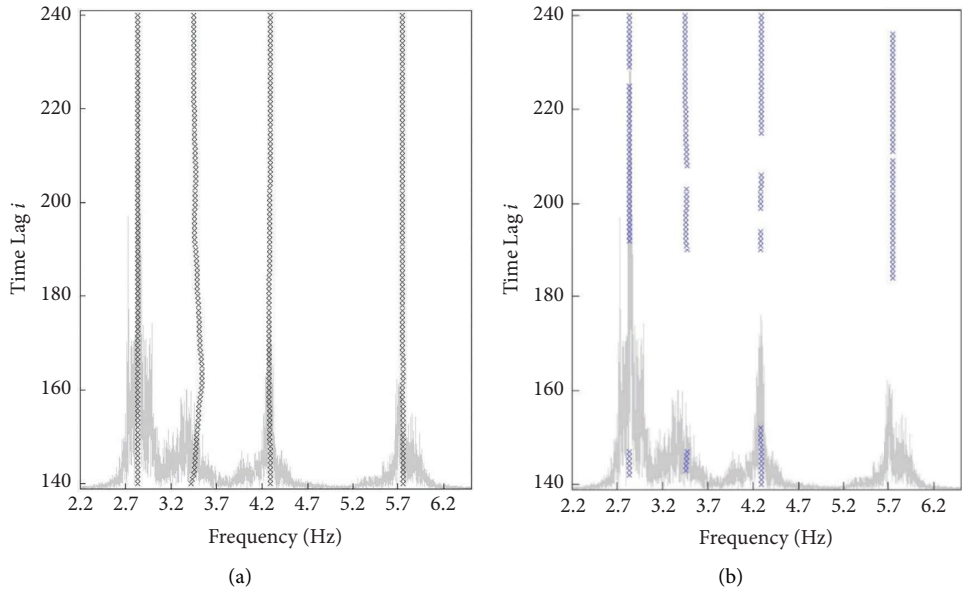

Figure 6: Alternative stabilization diagrams for SSI analysis of Cable 201b before and after the first sifting stage. (a) Before the first sifting stage. (b) After the first sifting stage.

effect of the flexural rigidity is relatively trivial) is exploited in this study to tackle the above difficulty. In other words, the ratio between any two obtained frequency values after the SSI analysis can be checked to systematically determine whether a frequency value is associated with a cable mode or not. Taking again Cables 107 and 201b as examples, the targets for both cases are similarly the three consecutive frequencies from the second to the fourth mode (F_2, F_3, and F_4) as mentioned in Section 3.2. Thus, it should be feasible to efficiently sieve out the red dots in Figures 7 and 8 with a numerical algorithm based on the three conditions $F_4/F_2 \approx 2.0$, $F_4/F_3 \approx 1.333$, and $F_3/F_2 \approx 1.5$ from reasonable frequency ratios. Even if the situation for Cable 107 in the interval from 00:15 to 00:30 does occur, it is still not difficult to judge that the two remaining frequency values after the sieving algorithm belong to the second and third modes. Similarly, the other situation that occurred in the interval from 01:15 to 01:30 can also be well handled to confirm that the two sieved frequency values correspond to the third and fourth modes.

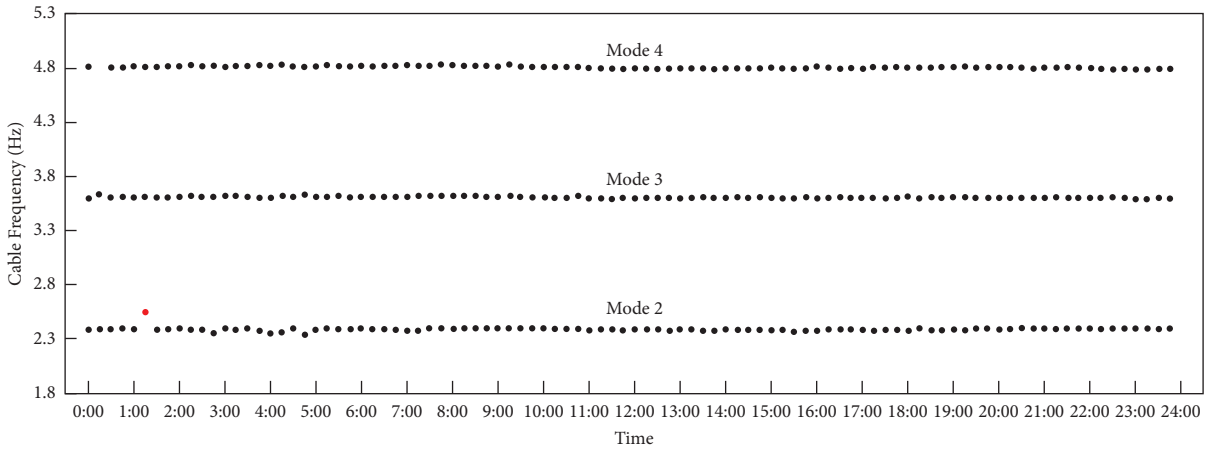

Figure 7: Results for the acceleration measurement of Cable 107 on 2020/10/21 after SSI analysis.

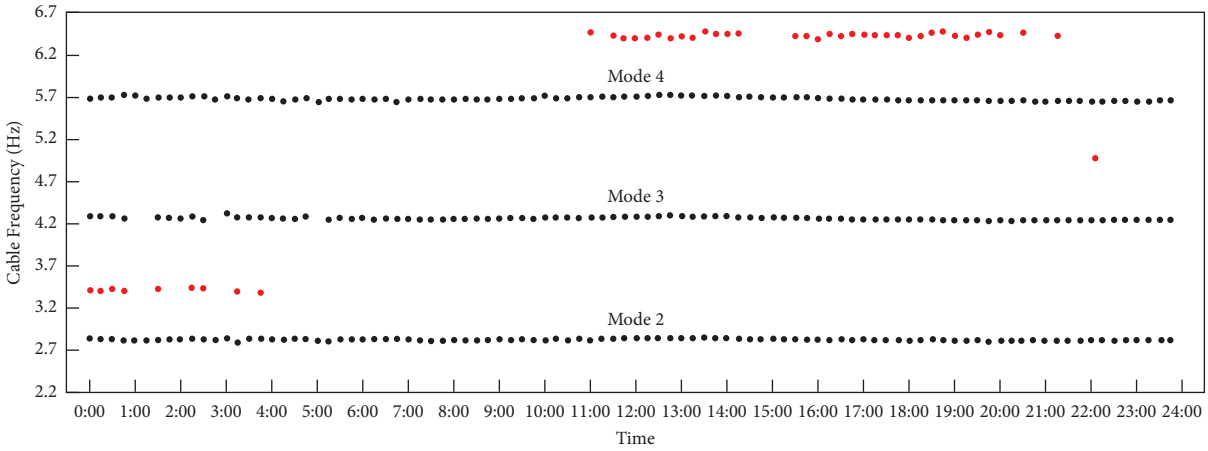

Figure 8: Results for the acceleration measurement of Cable 201b on 2020/10/22 after SSI analysis.

Overall, the SSI analysis reviewed in the previous section would be first performed on each interval of 15-minute cable acceleration measurement to obtain the identified frequency values at each interval. The sieving algorithm elaborated in this section is then applied to exclude the possibly occurring red dots as shown in Figures 7 and 8 and specify the mode orders corresponding to the cable frequencies remaining. Finally, the cable tension at each interval is calculated by equation (10) according to the prescribed mode priority order that will be discussed in the next section. For establishing an automatic algorithm, criteria on the ratios between frequency values are imposed with a threshold of tolerance δ determined from the statistical tests described in the next subsection. Furthermore, the extreme situations where only one frequency value is identified after the SSI analysis with no frequency ratio available are also considered in the current work. The solely identified frequency value in such cases will be compared with the average of each targeted cable frequency in a certain period (say, a week or a month). Another threshold of tolerance γ also decided by the statistical tests is additionally adopted to search for the corresponding mode under such circumstances. All details of the sieving algorithm will be given in the next subsection.

4.2. Detailed Descriptions of Algorithm. For the convenience of explanation, the whole automated sieving algorithm to extract reliable cable frequencies and determine their mode orders can be first illustrated with the flowchart for the mainstream process shown in Figure 9. This main flowchart also includes three branch processes whose flowcharts are displayed in Figures 10–12. If $m_1 < m_2 < m_3$ denote the three consecutive mode orders selected for each cable as listed in Table 2, the three corresponding theoretical frequency ratios can then be directly computed by $\alpha_{31} = m_3/m_1$, $\alpha_{32} = m_3/m_2$, and $\alpha_{21} = m_2/m_1$. As discussed in Section 3.3 and listed in Table 2, the assigned value of the system

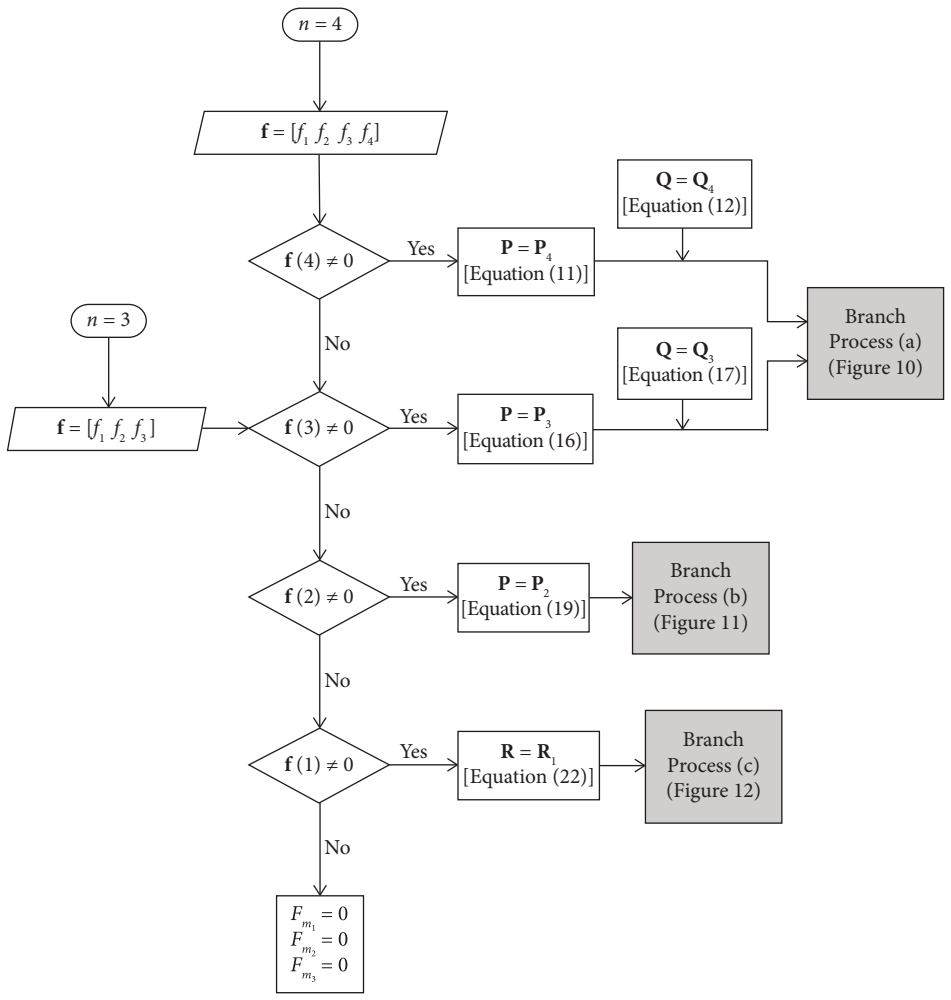

Figure 9: Flowchart for the mainstream process of automated sieving algorithm.

order parameter in conducting the SSI analysis for each cable can be either $n = 3$ or $n = 4$. That is to say, there are at most three identified frequency values after the SSI analysis when $n = 3$ or four when $n = 4$. Accordingly, two entrances corresponding to these two cases are designed for the main flowchart in Figure 9. In each time interval, assume that four frequency values $\mathbf{f} = [f_1 \ f_2 \ f_3 \ f_4]$ are identified when $n = 4$ and three frequency values $\mathbf{f} = [f_1 \ f_2 \ f_3]$ are obtained when $n = 3$, both arranged in an ascending order. If the number of identified frequency values is less than three for the case of $n = 3$ or less than four for the case of $n = 4$ in any interval, the last one or more elements in the vector $\mathbf{f}$ would be filled with the value zero to serve as an indicator for the subsequent automatic checking. No matter starting from the entrance for $n = 4$ or $n = 3$, the first step is always to input the identified frequency vector $\mathbf{f}$.

For the case of $n = 4$, the condition of $\mathbf{f}(4) \neq 0$ is first inspected to confirm the identification of four frequency values after conducting the SSI analysis for the considered time interval. If the answer is positive, the matrix

$$\mathbf{P}_4 = \begin{bmatrix} \mathbf{f}(4)/\mathbf{f}(1) & \mathbf{f}(4)/\mathbf{f}(1) & \mathbf{f}(4)/\mathbf{f}(1) \\ \mathbf{f}(4)/\mathbf{f}(2) & \mathbf{f}(4)/\mathbf{f}(2) & \mathbf{f}(4)/\mathbf{f}(2) \\ \mathbf{f}(4)/\mathbf{f}(3) & \mathbf{f}(4)/\mathbf{f}(3) & \mathbf{f}(4)/\mathbf{f}(3) \\ \mathbf{f}(3)/\mathbf{f}(1) & \mathbf{f}(3)/\mathbf{f}(1) & \mathbf{f}(3)/\mathbf{f}(1) \\ \mathbf{f}(3)/\mathbf{f}(2) & \mathbf{f}(3)/\mathbf{f}(2) & \mathbf{f}(3)/\mathbf{f}(2) \\ \mathbf{f}(2)/\mathbf{f}(1) & \mathbf{f}(2)/\mathbf{f}(1) & \mathbf{f}(2)/\mathbf{f}(1) \end{bmatrix} ./ \begin{bmatrix} \alpha_{31} & \alpha_{32} & \alpha_{21} \\ \alpha_{31} & \alpha_{32} & \alpha_{21} \\ \alpha_{31} & \alpha_{32} & \alpha_{21} \\ \alpha_{31} & \alpha_{32} & \alpha_{21} \\ \alpha_{31} & \alpha_{32} & \alpha_{21} \\ \alpha_{31} & \alpha_{32} & \alpha_{21} \end{bmatrix} - 1, \tag{11}$$

needs to be computed. In equation (11), ./ stands for the direct division operation taken between any two corresponding elements in two matrices with the same size and the last term "−1" means to subtract 1 from each element in a matrix, both coming from the syntax of the software MATLAB. With the design of equation (11), the six elements in each column of $\mathbf{P}_4$ would indicate the relative errors for all the six possible ratios produced by any two of the four identified frequency values compared with the theoretical frequency ratios α_{31} (the first column), α_{32} (the second column), or α_{21} (the third column). Moreover, the allocation matrix

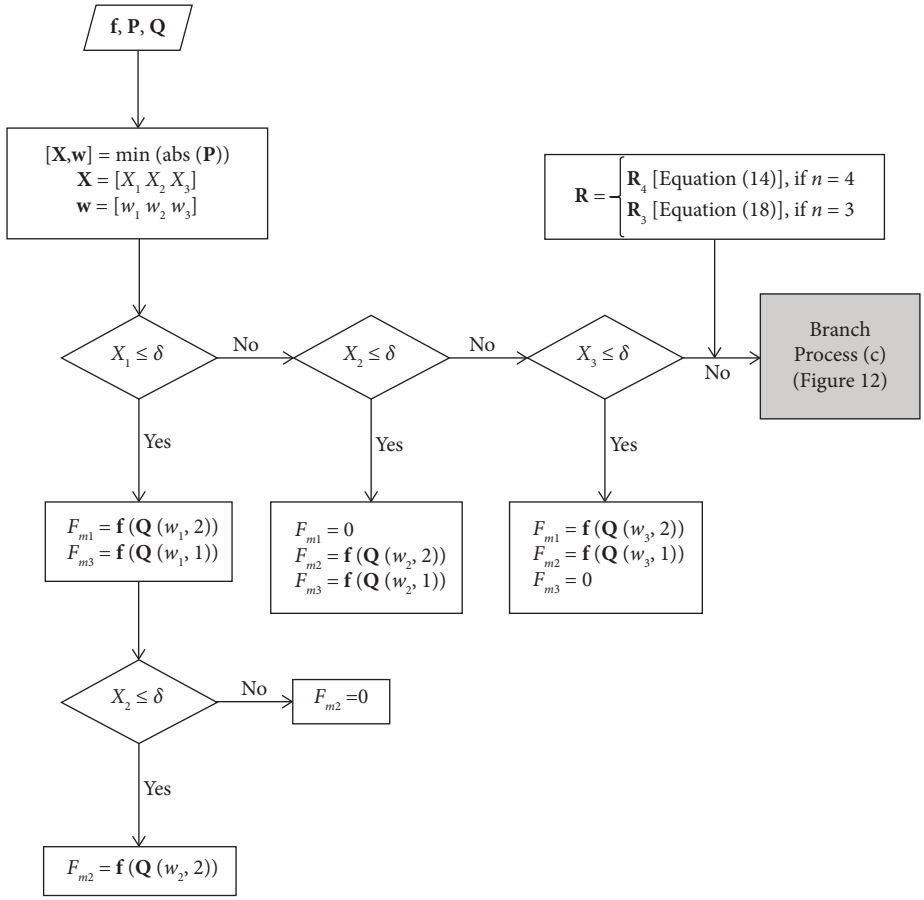

Figure 10: Flowchart for branch process (a) of automated sieving algorithm.

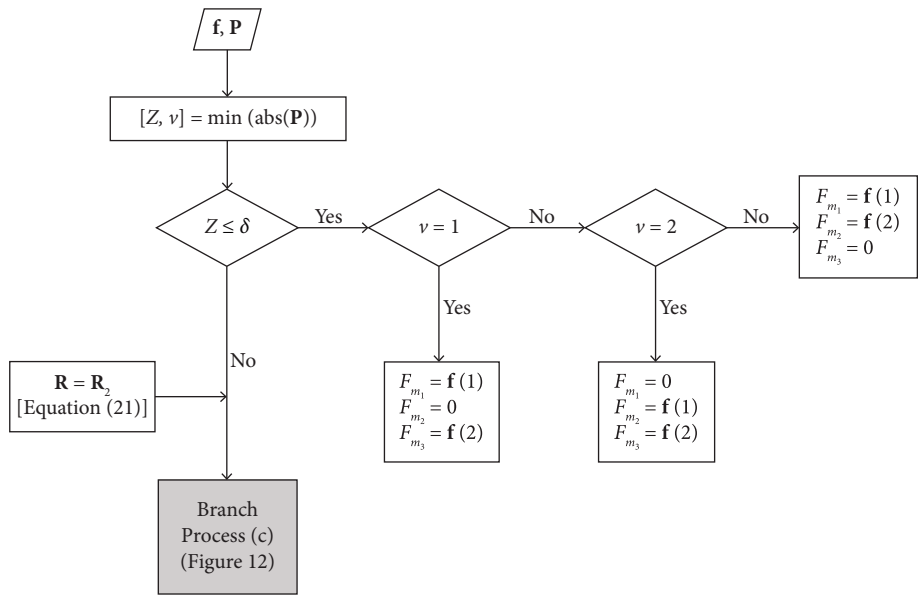

Figure 11: Flowchart for branch process (b) of automated sieving algorithm.

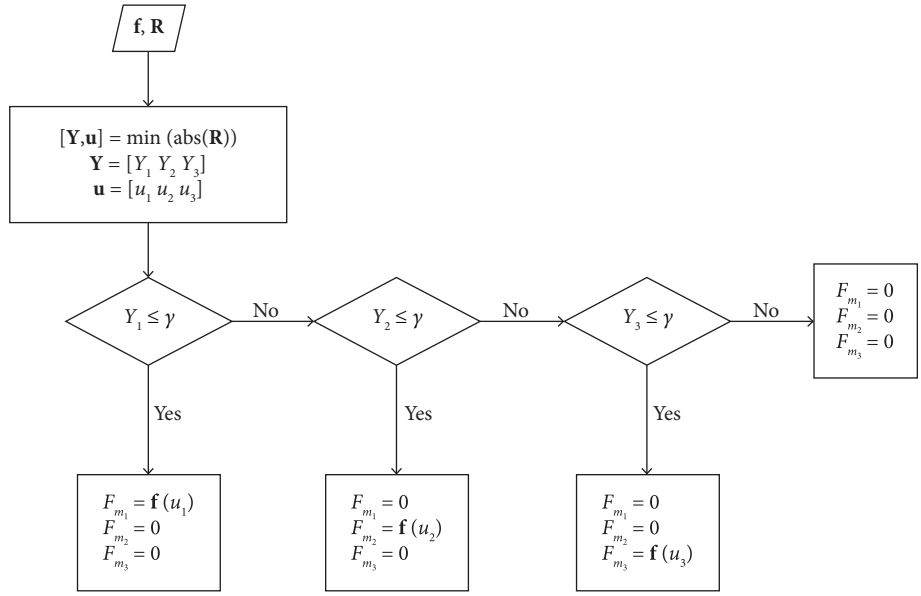

Figure 12: Flowchart for branch process (c) of automated sieving algorithm.

$$\mathbf{Q}_4 = \begin{bmatrix} 4 & 1 \\ 4 & 2 \\ 4 & 3 \\ 3 & 1 \\ 3 & 2 \\ 2 & 1 \end{bmatrix}, \tag{12}$$

associated with the arrangement of the six frequency ratios in equation (11) can also be defined and will be used later.

$\mathbf{P}_4$ and $\mathbf{Q}_4$ can be subsequently input into the branch process (a) as illustrated in Figure 10 to deal with the cases possessing four identified frequency values or three. When the four identified frequency values are confirmed, this branch process will first carry out the following operation on $\mathbf{P}_4$:

$$[\mathbf{X}\,\mathbf{w}] = \min\left(\text{abs}\left(\mathbf{P}_4\right)\right). \tag{13}$$

This operation takes the absolute value for each element in $\mathbf{P}_4$ and then stores the minimum value of each column at $\mathbf{X} = [X_1\ X_2\ X_3]$ together with recording the row positions of these minimum values at $\mathbf{w} = [w_1\ w_2\ w_3]$. It should be particularly noted that X_1, X_2, and X_3 actually represent the smallest relative errors for the frequency ratios compared to α_{31}, α_{32}, and α_{21}, respectively. Hence, sequential inspection on whether X_1, X_2, or X_3 exceeds the threshold of tolerance δ as schemed in Figure 10 would explicitly discriminate which three or which two identified values are cable frequencies. With the help of the allocation matrix $\mathbf{Q}_4$, the corresponding mode orders for these cable frequencies can also be handily matched to output the determined cable frequencies F_{m_1}, F_{m_2}, and F_{m_3}. A zero value for any of these output cable frequencies would imply that no identified value can correspond to that mode.

But if X_1, X_2, and X_3 all go beyond δ, then there is at most one among the four identified values to be possibly taken as the modal frequency of the cable and this part of sieving is handled by the branch process (c) demonstrated in Figure 12. Under such circumstances, the check of frequency ratios would not provide any useful information and the only left approach may be to compare with the reference values of cable frequencies. This research adopts the average frequency values $\overline{F}_{m_1}$, $\overline{F}_{m_2}$, and $\overline{F}_{m_3}$ for the three selected modes in the past one week to serve as the reference. By computing the matrix

$$\mathbf{R}_4 = \begin{bmatrix} \mathbf{f}(1) & \mathbf{f}(1) & \mathbf{f}(1) \\ \mathbf{f}(2) & \mathbf{f}(2) & \mathbf{f}(2) \\ \mathbf{f}(3) & \mathbf{f}(3) & \mathbf{f}(3) \\ \mathbf{f}(4) & \mathbf{f}(4) & \mathbf{f}(4) \end{bmatrix} ./ \begin{bmatrix} \overline{F}_{m_1} & \overline{F}_{m_2} & \overline{F}_{m_3} \\ \overline{F}_{m_1} & \overline{F}_{m_2} & \overline{F}_{m_3} \\ \overline{F}_{m_1} & \overline{F}_{m_2} & \overline{F}_{m_3} \\ \overline{F}_{m_1} & \overline{F}_{m_2} & \overline{F}_{m_3} \end{bmatrix} - 1, \tag{14}$$

the four elements in each column of $\mathbf{R}_4$ would indicate the relative errors for the four identified frequency values compared with the average frequency value of each selected mode. $\mathbf{R}_4$ is then input into the branch process (c) to perform the following operation:

$$\left[\mathbf{Y}\ \ \mathbf{u}\right] = \min\left(\text{abs}\left(\mathbf{R}_4\right)\right). \tag{15}$$

Similar to equation (13), equation (15) takes the absolute value for each element in $\mathbf{R}_4$, collects the minimum value of each column at $\mathbf{Y} = [Y_1\ Y_2\ Y_3]$, and also saves the row positions of these minimum values at $\mathbf{u} = [u_1\ u_2\ u_3]$. Again, Y_1, Y_2, and Y_3 obtained from equation (15) represent the smallest relative errors for the four identified frequency values compared to $\overline{F}_{m_1}$, $\overline{F}_{m_2}$, and $\overline{F}_{m_3}$, respectively. Sequential examination on whether Y_1, Y_2, or Y_3 is no larger than the threshold of tolerance γ as arranged in Figure 12

would find the only identified value to be qualified as a cable frequency and its corresponding mode. Such a value can then be output to the only appropriate choice among F_{m_1}, F_{m_2}, and F_{m_3}. The zero value is finally assigned to the other two left candidates.

In addition to the situation with four identified frequency values considered above, the circumstance with three identified frequency values after conducting the SSI analysis for the examined time interval will be discussed next. The occurrence of such a situation can be verified by satisfying $\mathbf{f}(4) = 0$ and $\mathbf{f}(3) \neq 0$ in the case of $n = 4$ or checking $\mathbf{f}(3) \neq 0$ in the case of $n = 3$. The branch process (a) in Figure 10 is also applicable if simply three frequency values are identified, but the inputs need to be replaced with

$$\mathbf{P}_3 = \begin{bmatrix} \mathbf{f}(3)/\mathbf{f}(1) & \mathbf{f}(3)/\mathbf{f}(1) & \mathbf{f}(3)/\mathbf{f}(1) \\ \mathbf{f}(3)/\mathbf{f}(2) & \mathbf{f}(3)/\mathbf{f}(2) & \mathbf{f}(3)/\mathbf{f}(2) \\ \mathbf{f}(2)/\mathbf{f}(1) & \mathbf{f}(2)/\mathbf{f}(1) & \mathbf{f}(2)/\mathbf{f}(1) \end{bmatrix} ./ \begin{bmatrix} \alpha_{31} & \alpha_{32} & \alpha_{21} \\ \alpha_{31} & \alpha_{32} & \alpha_{21} \\ \alpha_{31} & \alpha_{32} & \alpha_{21} \end{bmatrix} - 1, \tag{16}$$

and a new allocation matrix:

$$\mathbf{Q}_3 = \begin{bmatrix} 3 & 1 \\ 3 & 2 \\ 2 & 1 \end{bmatrix}. \tag{17}$$

The three elements in each column of $\mathbf{P}_3$ represent the relative errors for all possible three ratios produced by any two of the three identified frequency values compared with the theoretical frequency ratios α_{31}, α_{32}, and α_{21}. Furthermore, $\mathbf{R}_4$ defined in equation (14) has to be also substituted by

$$\mathbf{R}_3 = \begin{bmatrix} \mathbf{f}(1) & \mathbf{f}(1) & \mathbf{f}(1) \\ \mathbf{f}(2) & \mathbf{f}(2) & \mathbf{f}(2) \\ \mathbf{f}(3) & \mathbf{f}(3) & \mathbf{f}(3) \end{bmatrix} ./ \begin{bmatrix} \overline{F}_{m_1} & \overline{F}_{m_2} & \overline{F}_{m_3} \\ \overline{F}_{m_1} & \overline{F}_{m_2} & \overline{F}_{m_3} \\ \overline{F}_{m_1} & \overline{F}_{m_2} & \overline{F}_{m_3} \end{bmatrix} - 1, \tag{18}$$

when it is necessary to enter the branch process (c) in Figure 12 for dealing with the sieving of only one possible cable frequency.

As for the situation with only two identified frequency values after the SSI analysis, its appearance can be detected if $\mathbf{f}(4) = \mathbf{f}(3) = 0$ and $\mathbf{f}(2) \neq 0$ in the case of $n = 4$ or if $\mathbf{f}(3) = 0$ and $\mathbf{f}(2) \neq 0$ in the case of $n = 3$. The branch process (b) in Figure 11 is designed for such a circumstance and requires an even simpler input matrix:

$$\mathbf{P}_2 = \begin{bmatrix} \mathbf{f}(2)/\mathbf{f}(1) & \mathbf{f}(2)/\mathbf{f}(1) & \mathbf{f}(2)/\mathbf{f}(1) \end{bmatrix} ./ \begin{bmatrix} \alpha_{31} & \alpha_{32} & \alpha_{21} \end{bmatrix} - 1. \tag{19}$$

The single element in each column of $\mathbf{P}_2$ indicates the relative error for the ratio of two identified frequency values compared with the theoretical frequency ratios α_{31}, α_{32}, and α_{21}. This branch process will first execute the following operation on $\mathbf{P}_2$:

$$\begin{bmatrix} Z & v \end{bmatrix} = \min\left(\mathrm{abs}\left(\mathbf{P}_2\right)\right), \tag{20}$$

i.e., taking the absolute value for each element in $\mathbf{P}_2$ and then storing the minimum value of all three elements at Z together with recording its original column position at v. The obtained value of Z represents the smallest relative error between the single frequency ratio and its closest partner among α_{31}, α_{32}, and α_{21}. If the condition check of $Z \leq \delta$ is positive, it means that the two identified values would correspond to two cable frequencies. Further with the value of v, these two cable frequencies can find their corresponding mode orders and are output to the appropriate two of F_{m_1}, F_{m_2}, and F_{m_3}. A zero value will also be assigned to the remaining one without any correspondence. If the value of Z exceeds the tolerance δ, on the other hand, then at most one of the two identified values is possibly regarded as a cable frequency and this part of sieving can again be conducted by the branch process (c) in Figure 12. But in this case, the input should be changed as

$$\mathbf{R}_2 = \begin{bmatrix} \mathbf{f}(1) & \mathbf{f}(1) & \mathbf{f}(1) \\ \mathbf{f}(2) & \mathbf{f}(2) & \mathbf{f}(2) \end{bmatrix} ./ \begin{bmatrix} \overline{F}_{m_1} & \overline{F}_{m_2} & \overline{F}_{m_3} \\ \overline{F}_{m_1} & \overline{F}_{m_2} & \overline{F}_{m_3} \end{bmatrix} - 1, \tag{21}$$

which is similar to $\mathbf{R}_4$ defined in equation (14) and $\mathbf{R}_3$ defined in equation (18) but designed to manage the case with two identified frequency values.

Finally, consider the case where only one frequency value can be identified from the SSI analysis. The occurrence of this situation would be associated with $\mathbf{f}(4) = \mathbf{f}(3) = \mathbf{f}(2) = 0$ as well as $\mathbf{f}(1) \neq 0$ when $n = 4$ or $\mathbf{f}(3) = \mathbf{f}(2) = 0$ as well as $\mathbf{f}(1) \neq 0$ when $n = 3$. The branch process (c) in Figure 12 is also applicable in this case but requires a new input matrix:

$$\mathbf{R}_1 = \begin{bmatrix} \mathbf{f}(1) & \mathbf{f}(1) & \mathbf{f}(1) \end{bmatrix} ./ \begin{bmatrix} \overline{F}_{m_1} & \overline{F}_{m_2} & \overline{F}_{m_3} \end{bmatrix} - 1. \tag{22}$$

In the automatic sieving algorithm consisting of the mainstream process of Figure 9 and the three branch processes of Figures 10–12, the selection of the tolerances δ and γ also plays a pivoting role for its success in long-term SHM. It is always a great challenge to oscillate between a conservative choice that may mistakenly sieve out the modal frequencies of the cable and a loose criterion that could fail to effectively exclude a few unqualified frequency values. For a more reasonable determination of the thresholds of tolerance δ and γ, a trial value of 5% is first assigned for both to conduct the proposed sieving algorithm after carrying out the SSI analysis on the cable measurements from 2020/10/21 to 2020/10/27. The maximum and minimum values for the relative errors of the three sieved frequency ratios F_{m_3}/F_{m_1}, F_{m_3}/F_{m_2}, and F_{m_2}/F_{m_1} with respect to their corresponding mode order ratios α_{31}, α_{32}, and α_{21} in one week are arranged in Table 3 for the cables in the first two cable planes. Besides, similar statistics for the relative errors of the three sieved cable frequencies F_{m_1}, F_{m_2}, and F_{m_3} with respect to their corresponding weekly average values $\overline{F}_{m_1}$, $\overline{F}_{m_2}$, and $\overline{F}_{m_3}$ are also listed in Table 4. More specifically, Tables 3 and 4 are prepared to testify the legitimacy of the choices of δ and γ, respectively. It is evident from both tables that there are rather few cases to hold the relative errors slightly larger than 3% and these values are highlighted with

Table 3: Relative errors of sieved frequency ratios for cables in the first two cable planes.

Cable number	$(F_{m_3}/F_{m_1})/\alpha_{31} - 1$ (%)		$(F_{m_3}/F_{m_2})/\alpha_{32} - 1$ (%)		$(F_{m_2}/F_{m_1})/\alpha_{21} - 1$ (%)	
	Maximum	Minimum	Maximum	Minimum	Maximum	Minimum
101a	0.21	−1.07	0.58	−2.37	2.12	−1.09
101b	0.88	−0.90	1.99	−2.02	2.26	−2.04
102	0.44	−1.04	0.31	−0.48	0.54	−0.85
103	0.71	−1.41	1.86	−0.74	0.78	−2.48
104	0.83	−1.69	0.99	−1.06	2.51	−2.70
105	0.47	−0.38	0.93	−0.32	0.29	−1.03
106	0.50	−0.85	1.05	−0.19	0.30	−1.02
107	2.81	−0.53	0.66	−0.68	**3.46**	−0.39
108	2.97	−0.63	1.02	−2.45	**4.28**	−0.27
201a	2.97	−0.31	2.83	−1.11	2.46	−2.79
201b	2.75	−0.18	2.04	−1.53	2.90	−0.84
202	0.89	−0.44	0.56	−0.08	0.94	−0.43
203	2.96	−1.45	1.34	−0.88	**3.16**	−1.27
204	0.83	−2.85	0.85	−0.48	0.62	**−3.24**
205	1.87	−1.38	0.56	−0.55	1.86	−1.27
206	0.91	−0.45	1.28	−0.21	0.25	−1.13
207	**3.00**	−1.11	1.73	−0.26	2.59	−1.00
208	2.14	−2.78	1.82	−2.60	2.15	−1.35

Table 4: Relative errors of sieved cable frequencies for cables in the first two cable planes.

Cable number	$F_{m_1}/\overline{F}_{m_1} - 1$ (%)		$F_{m_2}/\overline{F}_{m_2} - 1$ (%)		$F_{m_3}/\overline{F}_{m_3} - 1$ (%)	
	Maximum	Minimum	Maximum	Minimum	Maximum	Minimum
101a	0.72	−0.88	1.80	−1.68	1.01	−1.19
101b	0.77	−1.10	1.91	−2.31	0.72	−0.88
102	1.58	−1.85	1.25	−1.79	1.31	−1.75
103	2.12	**−3.42**	2.33	−2.49	2.39	−2.98
104	2.10	−2.63	0.81	−1.72	0.36	−0.38
105	0.73	−0.44	0.66	−0.73	0.64	−0.51
106	0.92	−0.60	0.33	−0.80	0.51	−0.70
107	1.14	−2.15	0.96	−0.73	0.64	−0.85
108	1.50	−2.24	2.24	−1.21	0.58	−0.90
201a	2.59	−1.98	2.47	**−3.53**	2.30	−1.50
201b	2.20	−2.33	2.45	−2.06	2.04	−1.41
202	0.96	−1.27	1.01	−1.28	0.97	−1.22
203	2.76	**−3.29**	1.91	−2.11	1.94	−2.41
204	**3.78**	−1.74	1.01	−1.68	1.08	−1.77
205	1.11	−1.63	0.75	−0.54	0.51	−0.52
206	0.55	−0.58	0.55	−0.64	0.73	−0.79
207	1.86	−2.53	0.86	−1.27	1.66	−1.58
208	2.10	−2.51	0.80	−1.99	2.00	**−3.18**

slanted bold numbers. This means that very limited frequency values will be further sieved out if both tolerances are lowered to 3%. In other words, $\delta = \gamma = 3\%$ should be an excellent choice that can keep a good balance between identification rate and frequency variation. Consequently, such thresholds are taken in the subsequent long-term monitoring of this study and the results reported in the next section would demonstrate its effectiveness.

With the automatic sieving algorithm developed in the current section, the complete analysis for one week of acceleration measurements from 2020/10/21 to 2020/10/27 is first conducted to investigate its applicability in all 36 stay cables of Mao-Luo-Hsi Bridge. Even though various types of sieving results can be observed, they all lucidly reflect the efficacy of the proposed algorithm. In the case of Cable 107 ($n = 3$) as illustrated in Figure 13, only four frequency values indicated by red dots are sieved out in one week and three cable frequencies can be typically obtained in most time intervals. Regarding the case of Cable 201b ($n = 4$) as plotted in Figure 14, a number of inappropriate frequency values denoted by red dots cannot pass the sieving algorithm and three cable frequencies are eventually yielded in the majority of time intervals. Another sieving type can be found in Figure 15 for Cable 104 ($n = 3$), where a few unqualified frequency values are excluded and two cable frequencies are finally attained in a greater part of instances. It is especially noteworthy that several values very close to the frequency of the first cable mode are removed

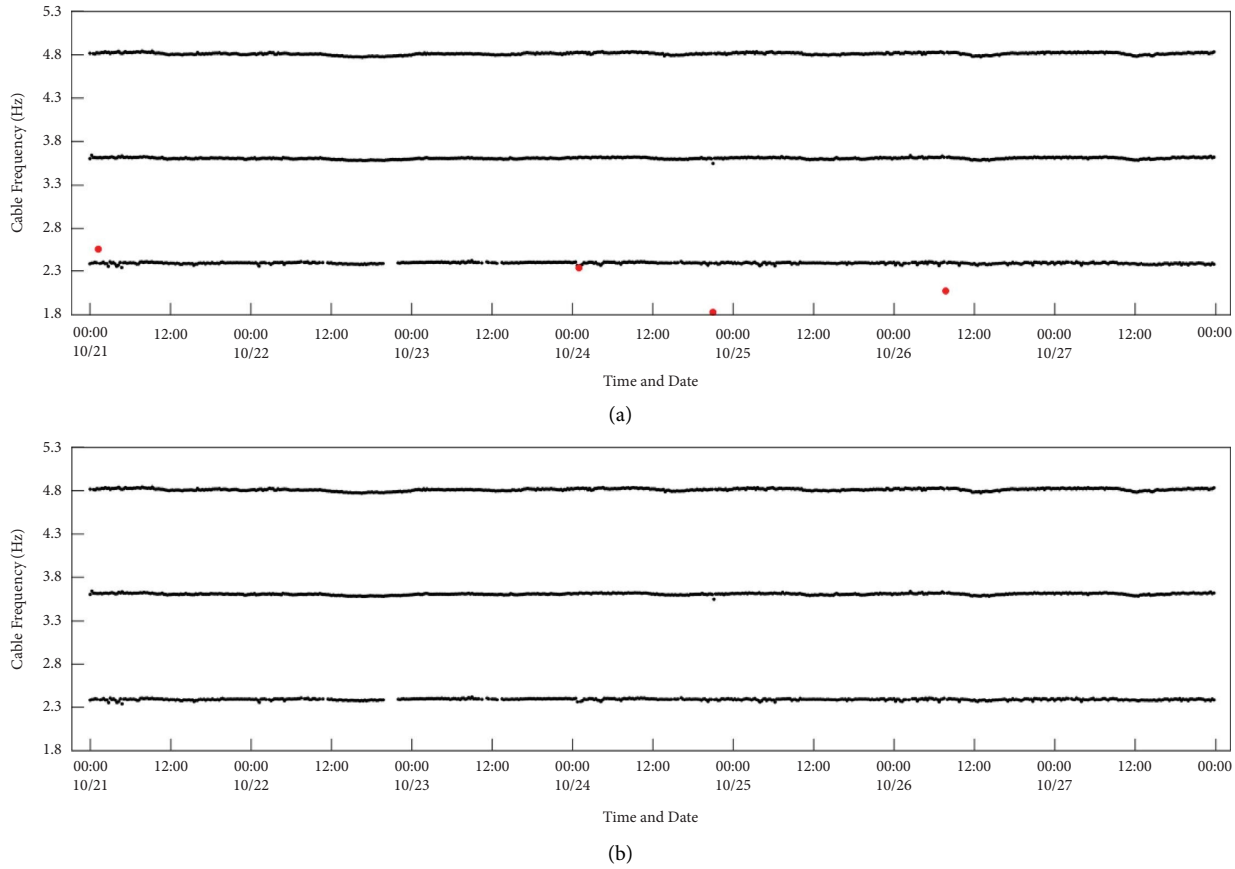

FIGURE 13: Variation of three selected modal frequencies for Cable 107 in one week. (a) Before automatic sieving. (b) After automatic sieving.

by the sieving algorithm in this case. Closer examination reveals that there are actually two identified frequency values from the SSI analysis for these time intervals to locate in the neighborhood of the fundamental frequency and one of them defeated by a narrow margin is appropriately sieved out by the algorithm. This can be directly recognized from the amplified illustration for the part near 00:00 of 10/23 in Figure 15(a).

5. Long-Term Monitoring Results of Cable Tension

Other than a reliable cable frequency identification methodology and an automated sieving algorithm as described in the previous two sections, the robustness of long-term cable tension monitoring may also rely on a proper choice of cable frequency to compute the tension value from equation (10). In this section, the priority order of cable frequencies for tension determination will be discussed in the first subsection, followed by presenting the cable tension monitoring results for a total of two years together with several observations in the second subsection.

5.1. Priority Order of Cable Frequencies for Tension Determination. In the current work, the decision of priority order in three target modes for each cable to compute the tension value is also based on one week of analyzed results from 2020/10/21 to 2020/10/27. For example, the identification rates for the sieved cable frequencies shown in Figures 13(b)–15(b) are reckoned and then ranked as graphed in Figure 16. Among all 672 15-minute measurements of Cable 107 in one week, 646 (96.1%) frequency values for the second mode, 672 (100%) for the third mode, and 671 (99.9%) for the fourth mode can be identified. Therefore, the priority order for Cable 107 is selected as Mode 3 (first), Mode 4 (second), and Mode 2 (third). Taking Cable 201b as another example, 671 (99.9%) frequency values for its second mode, 575 (85.6%) for its third mode, and 672 (100%) for its fourth mode can be obtained. According to these statistics, the priority order for Cable 201b is supposedly taken as Mode 4 (first), Mode 2 (second), and Mode 3 (third). But because the identification rates for Modes 2 and 4 are almost the same, the consideration of choosing lower modes whenever possible to reduce the influence of the flexural rigidity of the cable leads to the final

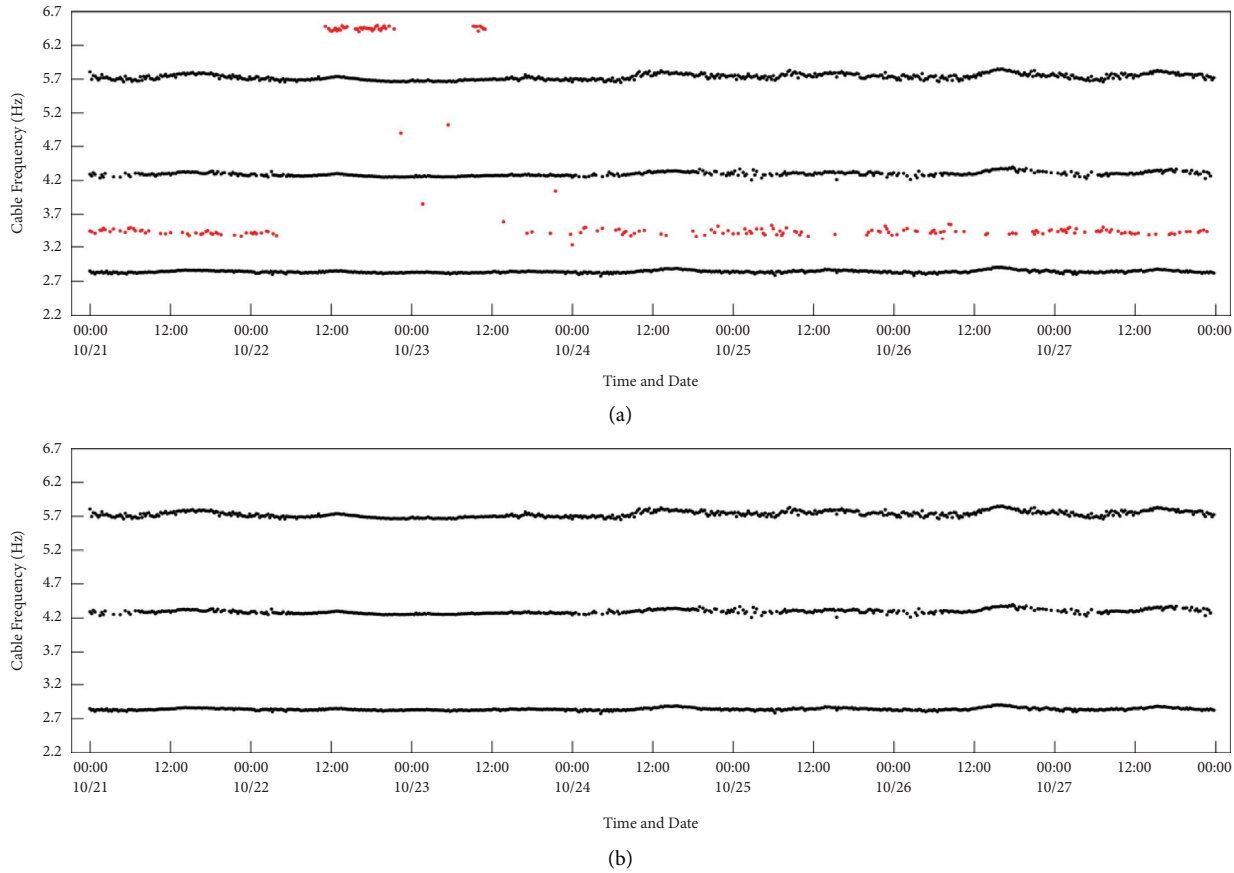

Figure 14: Variation of three selected modal frequencies for Cable 201b in one week. (a) Before automatic sieving. (b) After automatic sieving.

choice of Mode 2 (first), Mode 4 (second), and Mode 3 (third). The priority order of mode selection for all cables in the first two cable planes is also listed in Table 2.

According to the determined priority order, the tension value at each time interval can then be estimated with equation (10) using the mode with the highest priority. The tension histories of Cables 107, 201b, and 107 in one week are plotted in Figure 17 following from the sieved cable frequencies demonstrated in Figures 13(b)–15(b). From Figure 17, it is apparent that the tension values at all 672 time intervals can be consistently acquired and they all fall in a reasonable range of variation for each cable. It can be further observed that there exist different tendencies of variation for these three cables. For Cable 201b, its tension variation in one week can reach 30 tons (about 10%) and the daily maximum normally occurs during the daytime. This suggests that live load may be a dominant factor to induce the tension variation of a main cable like Cable 201b in this bridge. Regarding Cable 104, its weekly tension variation is only restricted to 7 tons (around 5%) and the daily minimum clearly happens at the daytime. In this case, temperature may be a crucial environmental factor to cause the change of cable tension, which is also supported by the smoother trend of variation. As for Cable 107, its tension variation in one week is also limited and shows no strong clues for the main influencing factor.

5.2. Long-Term Results of Cable Tension and Observations. Combining the previously reported anomaly processing algorithm [47] and the robust tension determination algorithm developed in this study, a real-time monitoring system for cable tension has officially started its operation on Mao-Luo-Hsi Bridge since 2020/11/1. It has lasted for more than two years so far. To convincingly verify the effectiveness of this monitoring system, the monitored tension histories of Cables 107, 201b, and 104 from 2020/11/01 to 2022/10/31 are comprehensively displayed in Figure 18. It can be evidently seen that reliable daily and long-term variations in cable tension are steadily obtained in real time for 24 months except for a duration of around 7 days in August of 2022 due to a problem of firmware. Similar to the trend observed in Figure 17 for one week, the long-term tension variation of Cable 201b is also noticeably greater than those of Cables 107 and 104. Moreover, the long-term tension variation of Cable 104 undoubtedly exhibits its yearly minimum in summer and yearly maximum in winter. Such a phenomenon further endorses that temperature is the major source to induce the tension variation of Cable 104.

To more extensively examine the practical performance of the real-time monitoring system for cable tension presented in the current work, the detailed statistics of tension monitoring for cables in the first two cable planes of Mao-Luo-Hsi Bridge in two full years are

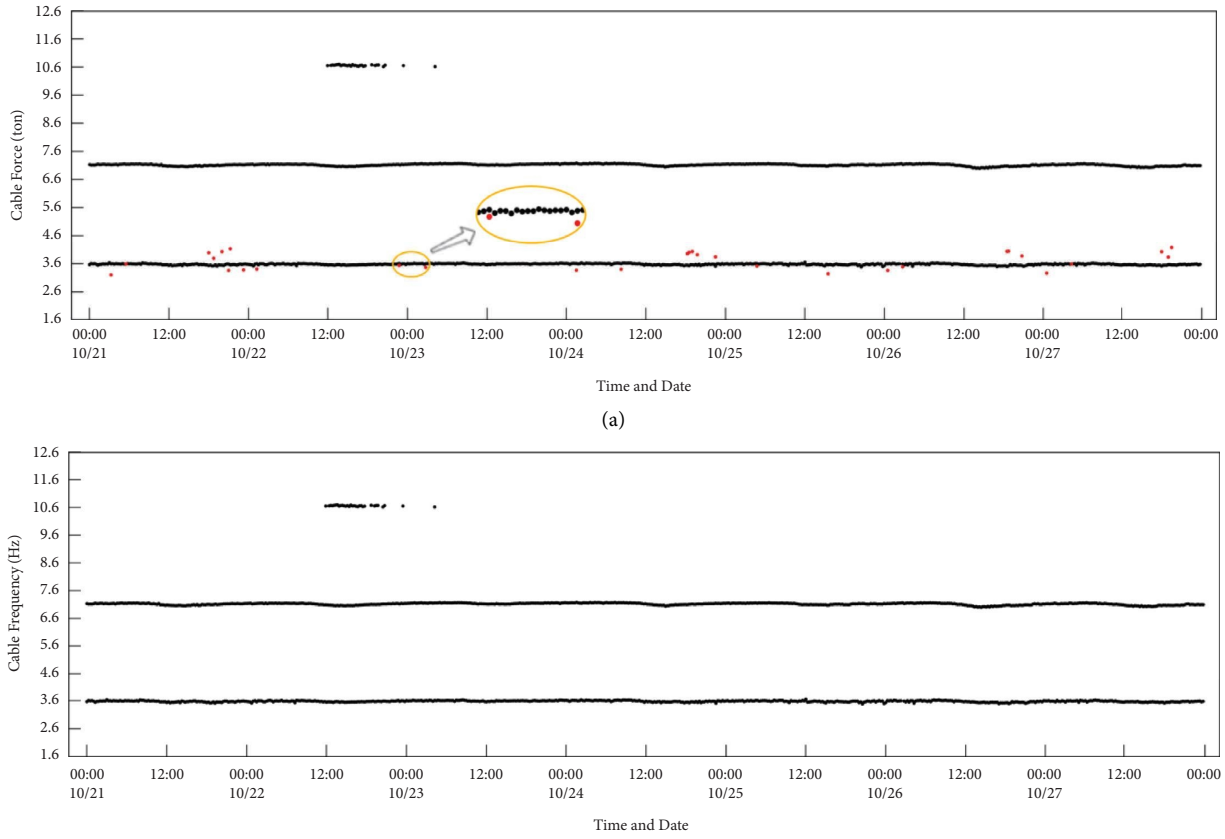

FIGURE 15: Variation of three selected modal frequencies for Cable 104 in one week. (a) Before automatic sieving. (b) After automatic sieving.

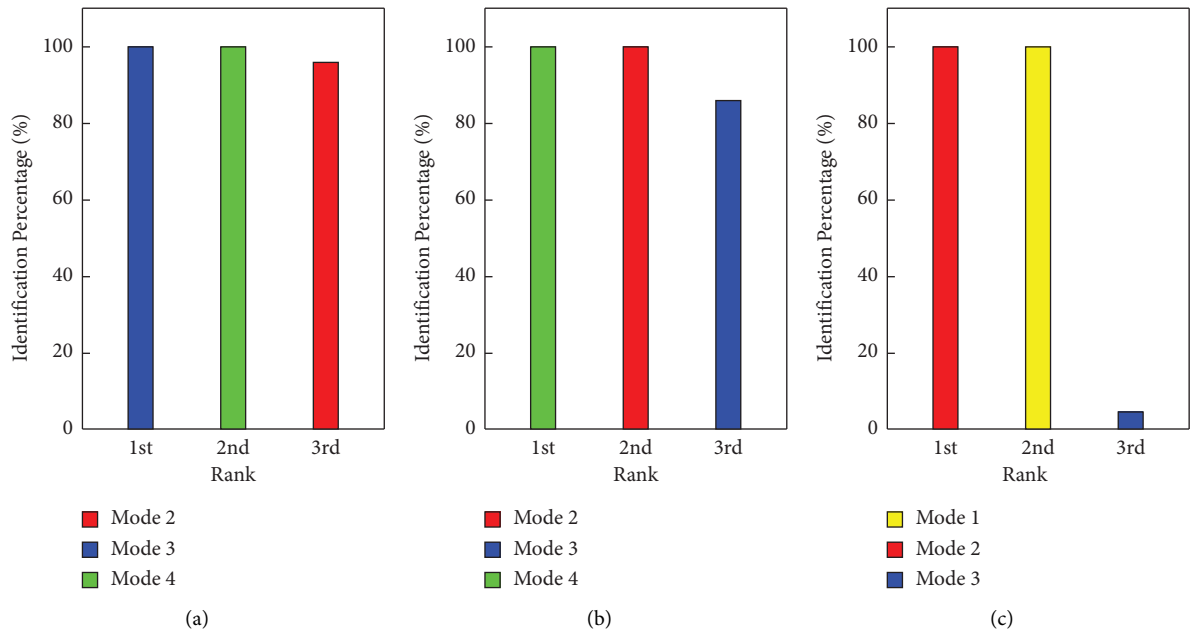

FIGURE 16: Identification percentages of the three target modes for three cables in one week. (a) Cable 107. (b) Cable 201b. (c) Cable 104.

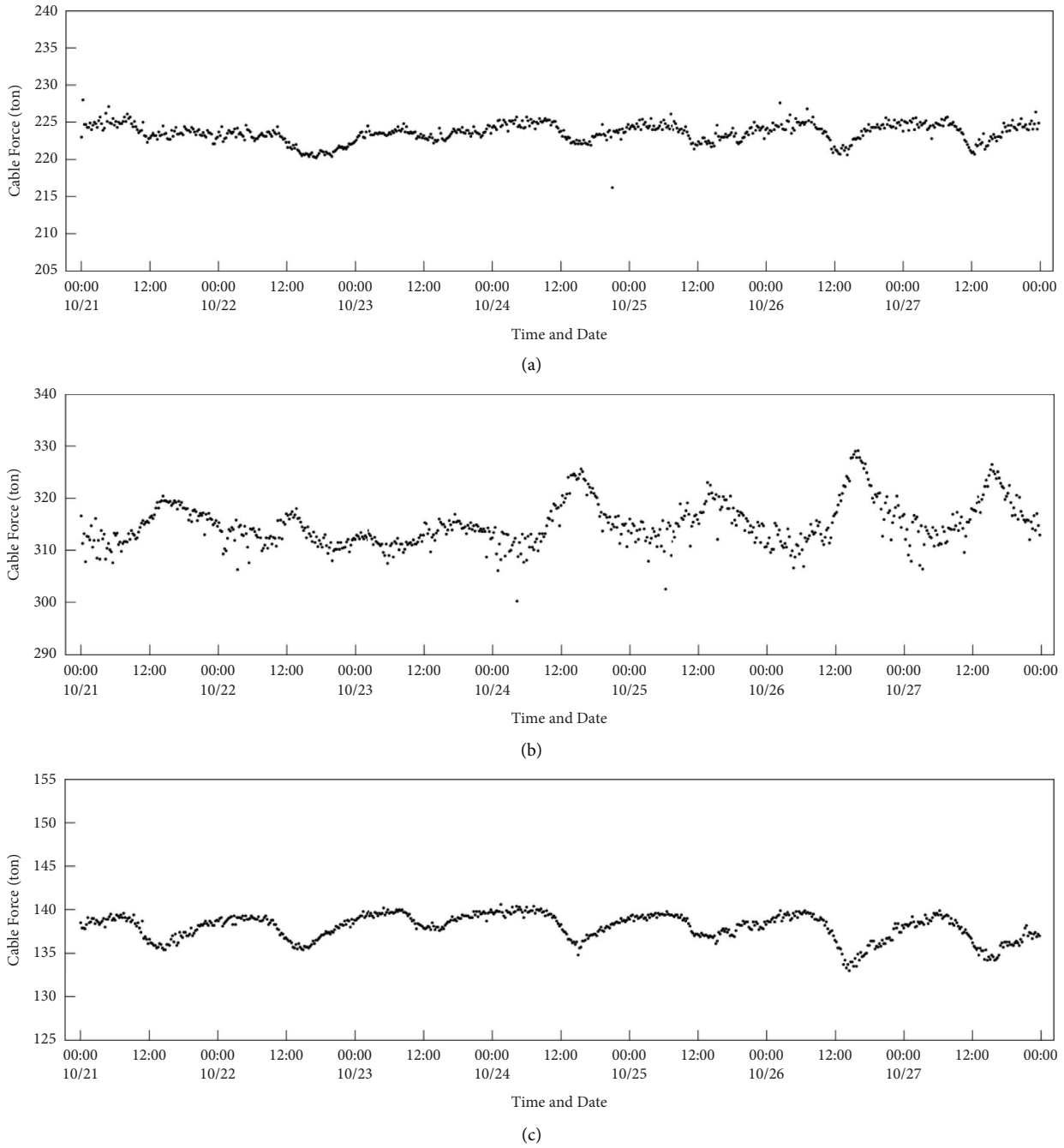

Figure 17: Tension histories of three cables in one week. (a) Cable 107. (b) Cable 201b. (c) Cable 104.

arranged in Table 5. There are totally 730 days from 2020/11/01 to 2022/10/31 such that 70080 15-minute measurement data files are potentially generated. The number of 15-minute time intervals with abnormal or no collected signals for each cable is first listed in Table 5. The reason for Cable 201a to have clearly more time intervals in this category is that the accelerometer installed on it together with the transmission wire was broken by strong winds in August of 2022 and had not been entirely repaired until the end of October. As for Cable 205, its extra data missing occurs in one period of around 5 days from 2021/9/4 to 2021/9/9 and another period of approximately 26 days from 2022/2/6 to 2022/3/4, both due to technical problems.

For each valid 15-minute measurement, the real-time monitoring system is applied to conduct tension estimation for the corresponding cable. Similar to the results plotted in Figure 18 for Cables 107, 201b, and 104, those of the other 15 cables also are found to be as successful. More specifically, the success rates for the determination of reliable tension in two years as long as the vibration signal is available are 100% for 15 among 18 cables in the first two planes. Even for the

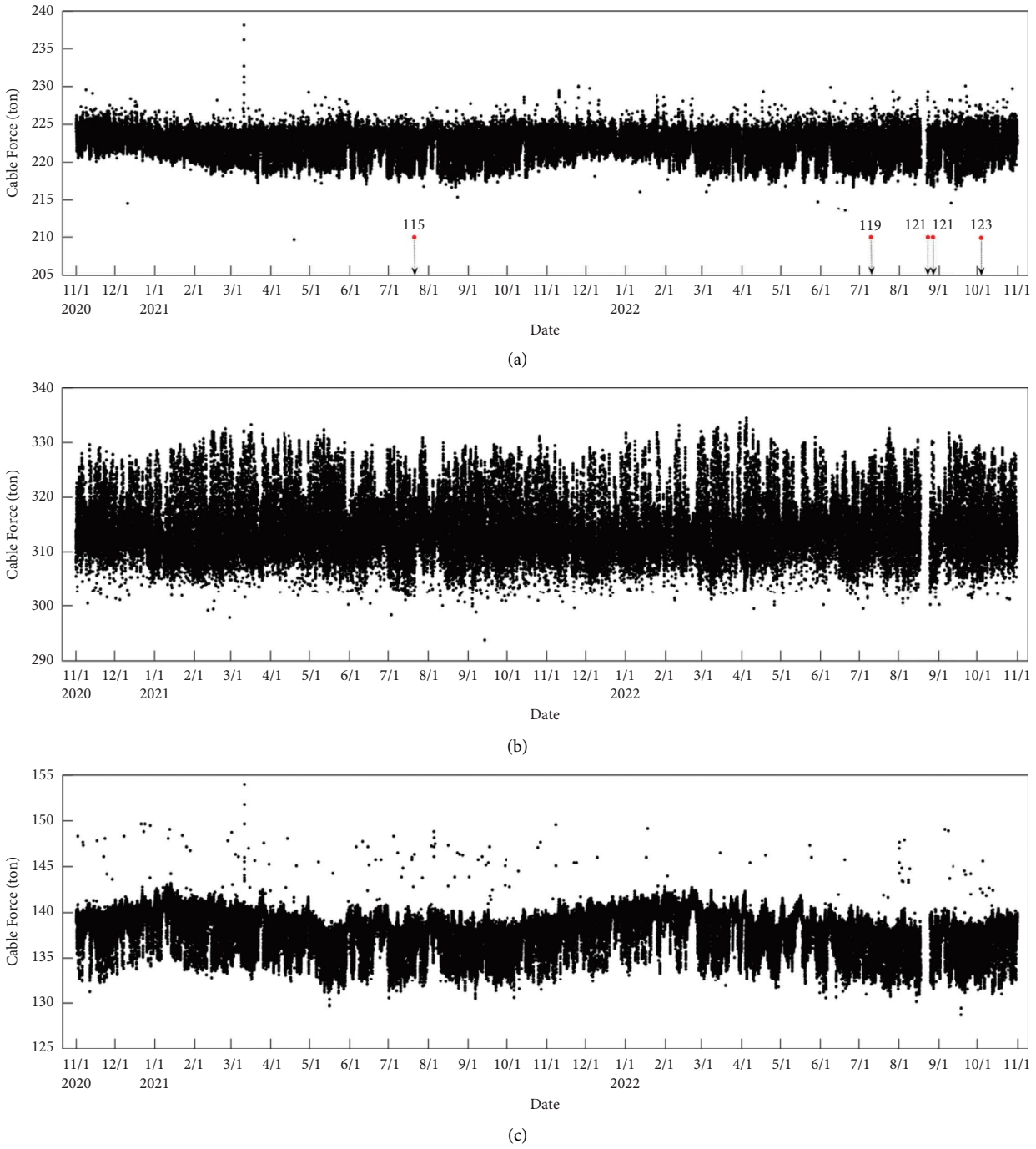

Figure 18: Tension histories of three cables for two years. (a) Cable 107. (b) Cable 201b, (c) Cable 104.

remaining three imperfect cases of Cables 107, 201a, and 208, the corresponding success rates all reach 99.99%. In the case of Cable 107, false tensions are obtained from the measurements in five time intervals, as illustrated by the red dots together with their clearly underestimated values in Figure 18(a). Taking the time interval from 01:00 to 01:15 of 2021/07/21 as an example, two frequency values 2.617 Hz and 3.533 Hz are obtained after the sifting stage of SSI analysis. As shown in Table 2, the target modes for Cable 107 are the 3rd, 4th, and 2nd modes in the order of priority. Since the ratio of the two obtained frequency values is 1.35 and very close to that for the cable frequencies of the 4th and 3rd modes, the automated sieving algorithm would consequently regard them as the cable frequencies of these two modes. However, 2.617 Hz is actually not a cable frequency and 3.533 Hz should correspond to the cable frequency of the 3rd mode. The tension value is eventually determined to be around 115 tons by mistakenly taking 2.617 Hz as the cable frequency of the 3rd mode. The other four false tension values are resulted from the same fault due to an erroneously sifted frequency value that happens to generate

Table 5: Statistics of tension monitoring for cables in the first two cable planes in two years.

Cable number	Number of 15-minute intervals							
	Total (a)	Abnormal or no signal (b)	No frequency from sieving algorithm	Tension determined from different mode priorities			False tension	Success rate (%) ($c + d + e/a - b$)
				1st (c)	2nd (d)	3rd (e)		
101a	$96 \times 365 \times 2 = 70080$	1211	0	68867	2	0	0	100.0
101b		1295	0	68782	3	0	0	100.0
102		1420	0	68660	0	0	0	100.0
103		1615	0	68461	4	0	0	100.0
104		1968	0	67976	136	0	0	100.0
105		2001	0	68079	0	0	0	100.0
106		2633	0	67404	39	4	0	100.0
107		2431	0	67610	30	4	**5**	**99.99**
108		2846	0	66764	458	12	0	100.0
201a		9197	**8**	60671	201	3	0	**99.99**
201b		3104	0	66900	76	0	0	100.0
202		3279	0	66801	0	0	0	100.0
203		3415	0	66467	198	0	0	100.0
204		3708	0	66363	9	0	0	100.0
205		6632	0	61910	1538	0	0	100.0
206		3950	0	66128	2	0	0	100.0
207		4146	0	65923	11	0	0	100.0
208		4323	0	64427	1328	1	**1**	**99.998**

an expected ratio with the merely available cable frequency. In fact, the only false tension observed in the case of Cable 208 is caused by the identical scenario. Even so, such a problem can be considered as a trivial defect of the proposed sieving algorithm based on fixed ratios of cable frequencies because it occurs in very rare and isolated occasions. Regarding the case of Cable 201a, there are eight time intervals in which no cable frequency can be identified by the sieving algorithm. Further inspection discloses that these intervals all fall between midnight and early morning. Particular weak vibration signals in situations with almost no traffic bring about this type of difficulty in the identification of cable frequencies.

From the statistics of mode priorities for each cable also listed in Table 5, it is clear that the tension values are overwhelmingly determined by the mode with the first priority in most cases for all the cables. Particularly for Cables 102, 105, and 202, all of their monitored tension values in two full years are decided by the most dominant mode. The mode with the second priority plays the most important role in the case of Cable 205 where the tension values of 1538 15-minute time intervals (2.4%) are calculated from this mode. As for the mode with the third priority, it appears on the stage only in the cases of 5 stay cables and is most active for Cable 108 where the tension values of 12 15-minute time intervals (0.02%) are obtained from this mode. Even though the marginal utility of including the third cable mode seems to be limited from these statistics, it should be especially noted that merely one frequency ratio would be available for the subsequent sieving algorithm if simply two cable frequencies are targeted in the identification process. Under such circumstances, the potential for the occurrence of false tension values as discussed in the previous paragraph may be substantially raised. On the other hand, the choice of more cable frequencies to further complicate the automatic sieving algorithm is also meaningless considering the excellent success rates of tension determination in all the examined cables. Accordingly, the selection of three cable frequencies as the identification target can be persuasively justified in the application of Mao-Luo-Hsi Bridge.

6. Conclusions

To develop a monitoring system of cable tension based on real-time vibration signals, this research first employs an efficient SSI method with tailored parameter selection to continuously identify the three frequencies of adjacent modes for the cables of Mao-Luo-Hsi Bridge. More importantly, an automated algorithm is delicately established to sieve out the stable modal frequencies by making the best of the specific modal frequency distribution for cables. The ratios between the frequency values identified from SSI analysis are exhaustively checked to systematically extract the qualified cable frequencies and decide their corresponding mode orders. The tension is finally computed with one available cable frequency according to the priority order predetermined by the statistics of identification rate. Overall, the current study achieves a real-time cable tension monitoring system by completing several imperative works in the analysis of long-term cable vibration signals, the selection of suitable parameters, the choice of balanced criteria, and the verification of proposed numerical procedures.

Demonstrated by analyzing the vibration signals measured from the stay cable of Mao-Luo-Hsi Bridge in real time for two full years, the effectiveness and robustness of this real-time monitoring system have been extensively testified. The success rates for the immediate determination of dependable tension are found to be perfect in two years for 15 of the 18 investigated cables. As for the other three cables, their corresponding success rates are still higher than 99.99% with eight cases of absent tension values due to very weak

signals and six cases of false tension values owing to the coincident sifting of a proportioned non-cable frequency value. Contrasting to the practical validation with relatively short durations of vibration measurements in other similar studies [38, 39], much more persuasive testimony has been provided for the real-time cable tension monitoring system developed in this work with such long-term results. Another interesting observation from these long-term cable tension histories of Mao-Luo-Hsi Bridge is that the tension variations of the main cables are usually more significant and possibly created by live load. On the other hand, the tension variations for other cables can be apparently more restricted and may be either influenced by temperature or without dominant environmental factors.

It is expected that the cable tension monitoring system currently applied in Mao-Luo-Hsi Bridge can be easily generalized to conduct real-time monitoring for the other cable-supported bridges with similar selections of parameters in the SSI analysis and the same automated sieving algorithm. Efforts are presently made to utilize the proposed methodology on another cable-stayed bridge and the other four arch bridges in Taiwan. The success in the application of Mao-Luo-Hsi Bridge, however, may be at least partly attributed to the high-quality measurements on its stay cables. This advantage keeps the cases with absent or false tension values to a minimum amount. If extended to the tension monitoring for the suspenders of arch bridges, the quality of the corresponding ambient vibration signals may be highly fluctuating and a few issues need to be more carefully explored. For example, the more frequent occurrence of coincidently proportioned frequency values as a result of inferior measurements in this case would deteriorate the flaw existing in the sieving algorithm to generate more false tension values. In fact, research work has been under way to further set up impeccable safety nets for the sieving algorithm under the interference of proportioned frequency values. Another effort attempting to utilize deep learning techniques such as the convolution neural network for replacing the sieving algorithm and increasing the application flexibility is also ongoing. It is hoped that these advanced works can be completed and reported in the near future.

Data Availability

The data used to support the findings of this study are available from the corresponding author upon request.

Conflicts of Interest

The authors declare that they have no conflicts of interest.

Acknowledgments

The authors are grateful for the financial support from National Science and Technology Council of Republic of China under grant nos. MOST108-2221-E-224-002-MY2 and MOST110-2221-E-224-007-MY3.

References

[1] J. C. Russell and T. J. Lardner, "Experimental determination of frequencies and tension for elastic cables," *Journal of Engineering Mechanics*, vol. 124, no. 10, pp. 1067–1072, 1998.

[2] A. Cunha, E. Caetano, and R. Delgado, "Dynamic tests on large cable-stayed bridge," *Journal of Bridge Engineering*, vol. 6, no. 1, pp. 54–62, 2001.

[3] W. X. Ren, H. L. Liu, and G. Chen, "Determination of cable tensions based on frequency differences," *Engineering Computations*, vol. 25, no. 2, pp. 172–189, 2008.

[4] M. A. Ceballos and C. A. Prato, "Determination of the axial force on stay cables accounting for their bending stiffness and rotational end restraints by free vibration tests," *Journal of Sound and Vibration*, vol. 317, no. 1-2, pp. 127–141, 2008.

[5] Z. Fang and J. Q. Wang, "Practical formula for cable tension estimation by vibration method," *Journal of Bridge Engineering*, vol. 17, no. 1, pp. 161–164, 2012.

[6] H. Zui, T. Shinke, and Y. Namita, "Practical formulas for estimation of cable tension by vibration method," *Journal of Structural Engineering*, vol. 122, no. 6, pp. 651–656, 1996.

[7] H. Nam and N. T. Nghia, "Estimation of cable tension using measured natural frequencies," *Procedia Engineering*, vol. 14, pp. 1510–1517, 2011.

[8] C. C. Chen, W. H. Wu, C. H. Huang, and G. Lai, "Determination of stay cable force based on effective vibration length accurately estimated from multiple measurements," *Smart Structures and Systems*, vol. 11, no. 4, pp. 411–433, 2013.

[9] C. C. Chen, W. H. Wu, M. R. Leu, and G. Lai, "Tension determination of stay cable or external tendon with complicated constraints using multiple vibration measurements," *Measurement*, vol. 86, pp. 182–195, 2016.

[10] W. H. Wu, C. C. Chen, Y. C. Chen, G. Lai, and C. M. Huang, "Tension determination for suspenders of arch bridge based on multiple vibration measurements concentrated at one end," *Measurement*, vol. 123, pp. 254–269, 2018.

[11] C. C. Chen, W. H. Wu, S. Y. Chen, and G. Lai, "A novel tension estimation approach for elastic cables by elimination of complex boundary condition effects employing mode shape functions," *Engineering Structures*, vol. 166, pp. 152–166, 2018.

[12] C. C. Chen, W. H. Wu, Y. T. Liu, and G. Lai, "A convenient cable tension estimation method simply based on local vibration measurements to fit partial mode shapes," *Engineering Structures*, vol. 272, Article ID 115008, 2022.

[13] B. Yan, J. Yu, and M. Soliman, "Estimation of cable tension force independent of complex boundary conditions," *Journal of Engineering Mechanics*, vol. 141, no. 1, Article ID 06014015, 2015.

[14] B. Yan, W. Chen, J. Yu, and X. Jiang, "Mode shape-aided tension force estimation of cable with arbitrary boundary conditions," *Journal of Sound and Vibration*, vol. 440, pp. 315–331, 2019.

[15] C. P. Yu, "Tension prediction for straight cables based on effective vibration length with a two-frequency approach," *Engineering Structures*, vol. 222, Article ID 111121, 2020.

[16] F. Magalhaes, A. Cunha, and E. Caetano, "Online automatic identification of the modal parameters of a long span arch bridge," *Mechanical Systems and Signal Processing*, vol. 23, no. 2, pp. 316–329, 2009.

[17] M. J. Whelan and K. D. Janoyan, "In-service diagnostics of a highway bridge from a progressive damage case study," *Journal of Bridge Engineering*, vol. 15, no. 5, pp. 597–607, 2010.

[18] M. W. Hackell and R. Rolfes, "Monitoring a 5 MW offshore wind energy converter – condition parameters and

triangulation based extraction of modal parameters," *Mechanical Systems and Signal Processing*, vol. 40, no. 1, pp. 322–343, 2013.

[19] D. Foti, V. Gattulli, and F. Potenza, "Output-only identification and model updating by dynamic testing in unfavorable conditions of a seismically damaged building," *Computer-Aided Civil and Infrastructure Engineering*, vol. 29, no. 9, pp. 659–675, 2014.

[20] F. Potenza, F. Federici, M. Lepidi, V. Gattulli, F. Graziosi, and A. Colarieti, "Long-term structural monitoring of the damaged Basilica S. Maria di Collemaggio through a low-cost wireless sensor network," *Journal of Civil Structural Health Monitoring*, vol. 5, no. 5, pp. 655–676, 2015.

[21] R. Mario Azzara, G. De Roeck, M. Girardi, C. Padovani, D. Pellegrini, and E. Reynders, "The influence of environmental parameters on the dynamic behaviour of the San Frediano bell tower in Lucca," *Engineering Structures*, vol. 156, pp. 175–187, 2018.

[22] Z. Q. Xiang, J. W. Pan, J. T. Wang, and F. D. Chi, "Improved approach for vibration-based structural health monitoring of arch dams during seismic events and normal operation," *Structural Control and Health Monitoring*, vol. 29, no. 7, Article ID e2955, 2022.

[23] M. Sun, Q. Li, and X. Han, "Investigation of long-term modal properties of a supertall building under environmental and operational variations," *Journal of Building Engineering*, vol. 62, Article ID 105439, 2022.

[24] K. Zhou, Q. S. Li, L. H. Zhi, X. L. Han, and K. Xu, "Investigation of modal parameters of a 600-m-tall skyscraper based on two-year-long structural health monitoring data and five typhoons measurements," *Engineering Structures*, vol. 274, Article ID 115162, 2023.

[25] Y. Zhang, M. Kurata, and J. P. Lynch, "Long-term modal analysis of wireless structural monitoring data from a suspension bridge under varying environmental and operational conditions: system design and automated modal analysis," *Journal of Engineering Mechanics*, vol. 143, no. 4, Article ID 04016124, 2017.

[26] J. X. Mao, H. Wang, Y. G. Fu, and B. F. Spencer, "Automated modal identification using principal component and cluster analysis: application to a long-span cable-stayed bridge," *Structural Control and Health Monitoring*, vol. 26, no. 10, Article ID e2430, 2019.

[27] M. Scionti and J. P. Lanslots, "Stabilisation diagrams: pole identification using fuzzy clustering techniques," *Advances in Engineering Software*, vol. 36, no. 11-12, pp. 768–779, 2005.

[28] E. P. Carden and J. M. Brownjohn, "Fuzzy clustering of stability diagrams for vibration-based structural health monitoring," *Computer-Aided Civil and Infrastructure Engineering*, vol. 23, no. 5, pp. 360–372, 2008.

[29] P. G. Bakir, "Automation of the stabilization diagrams for subspace based system identification," *Expert Systems with Applications*, vol. 38, no. 12, pp. 14390–14397, 2011.

[30] E. Reynders, J. Houbrechts, and G. De Roeck, "Fully automated (operational) modal analysis," *Mechanical Systems and Signal Processing*, vol. 29, no. 5, pp. 228–250, 2012.

[31] F. Ubertini, C. Gentile, and A. L. Materazzi, "Automated modal identification in operational conditions and its application to bridges," *Engineering Structures*, vol. 46, pp. 264–278, 2013.

[32] G. Zini, M. Betti, and G. Bartoli, "A quality-based automated procedure for operational modal analysis," *Mechanical Systems and Signal Processing*, vol. 164, Article ID 108173, 2022.

[33] G. Zonno, R. Aguilar, R. Boroschek, P. B. Lourenço, and P. B. Lourenco, "Automated long-term dynamic monitoring using hierarchical clustering and adaptive modal tracking: validation and applications," *Journal of Civil Structural Health Monitoring*, vol. 8, no. 5, pp. 791–808, 2018.

[34] J. Li, T. Bao, and C. E. Ventura, "An automated operational modal analysis algorithm and its application to concrete dams," *Mechanical Systems and Signal Processing*, vol. 168, Article ID 108707, 2022.

[35] A. Sadeqi, A. Esfandiari, M. Sanayei, and M. Rashvand, "Automated operational modal analysis based on long-term records: a case study of Milad Tower structural health monitoring," *Structural Control and Health Monitoring*, vol. 29, no. 10, Article ID e3037, 2022.

[36] M. Sun, M. M. Alamdari, and H. Kalhori, "Automated operational modal analysis of a cable-stayed bridge," *Journal of Bridge Engineering*, vol. 22, no. 12, Article ID 05017012, 2017.

[37] X. Zhang, W. Zhou, Y. Huang, and H. Li, "Automatic identification of structural modal parameters based on density peaks clustering algorithm," *Structural Control and Health Monitoring*, vol. 29, no. 12, Article ID e3138, 2022.

[38] Y. Yang, S. Li, S. Nagarajaiah, H. Li, and P. Zhou, "Real-time output-only identification of time-varying cable tension from accelerations via complexity pursuit," *Journal of Structural Engineering*, vol. 142, no. 1, Article ID 04015083, 2016.

[39] J. X. Li, T. H. Yi, C. X. Qu, H. N. Li, and H. Liu, "Adaptive identification of time-varying cable tension based on improved variational mode decomposition," *Journal of Bridge Engineering*, vol. 27, no. 8, Article ID 04022064, 2022.

[40] D. Jana, S. Nagarajaiah, and Y. Yang, "Computer vision-based real-time cable tension estimation algorithm using complexity pursuit from video and its application in Fred-Hartman cable-stayed bridge," *Structural Control and Health Monitoring*, vol. 29, no. 9, Article ID e2985, 2022.

[41] S. S. Jin, S. Jeong, S. H. Sim, D. W. Seo, and Y. S. Park, "Fully automated peak-picking method for an autonomous stay-cable monitoring system in cable-stayed bridges," *Automation in Construction*, vol. 126, Article ID 103628, 2021.

[42] S. Jeong, H. Kim, J. Lee, and S. H. Sim, "Automated wireless monitoring system for cable tension forces using deep learning," *Structural Health Monitoring*, vol. 20, no. 4, pp. 1805–1821, 2021.

[43] W. H. Wu, S. W. Wang, C. C. Chen, and G. Lai, "Application of stochastic subspace identification for stay cables with an alternative stabilization diagram and hierarchical sifting process," *Structural Control and Health Monitoring*, vol. 23, no. 9, pp. 1194–1213, 2016.

[44] W. H. Wu, S. W. Wang, C. C. Chen, and G. Lai, "Mode identifiability of a cable-stayed bridge under different excitation conditions assessed with an improved algorithm based on stochastic subspace identification," *Smart Structures and Systems*, vol. 17, no. 3, pp. 363–389, 2016.

[45] W. H. Wu, S. W. Wang, C. C. Chen, and G. Lai, "Assessment of environmental and non-destructive earthquake effects on modal parameters of an office building based on long-term vibration measurements," *Smart Materials and Structures*, vol. 26, no. 5, Article ID 055034, 2017.

[46] W. H. Wu, J. W. Jhou, C. C. Chen, and G. Lai, "A novel recursive stochastic subspace identification algorithm with its application in long-term structural health monitoring of office buildings," *Smart Structures and Systems*, vol. 24, no. 4, pp. 459–474, 2019.

[47] W. H. Wu, C. C. Chen, S. L. Lin, and G. Lai, "Automatic anomaly detection and processing for long-term tension monitoring of stay cables based on vibration measurements," *Intelligent Transportation Infrastructure*, vol. 1, no. 1, pp. 1–10, 2022.

[48] W. H. Wu, S. W. Wang, C. C. Chen, and G. Lai, "Modal parameter identification for closely spaced modes of civil structures based on an upgraded stochastic subspace methodology," *Structure and Infrastructure Engineering*, vol. 15, no. 3, pp. 296–313, 2019.